catalysts

MDPI

Review

Ultrasonic Monitoring of Biocatalysis in Solutions and Complex Dispersions

Vitaly Buckin * and Margarida Caras Altas

School of Chemistry, University College Dublin, Belfield, Dublin 4, Ireland; maguy.ca@gmail.com
* Correspondence: vitaly.buckin@ucd.ie; Tel.: +353-1-7162371

Received: 19 September 2017; Accepted: 26 October 2017; Published: 15 November 2017

Abstract: The rapidly growing field of chemical catalysis is dependent on analytical methods for non-destructive real-time monitoring of chemical reactions in complex systems such as emulsions, suspensions and gels, where most analytical techniques are limited in their applicability, especially if the media is opaque, or if the reactants/products do not possess optical activity. High-resolution ultrasonic spectroscopy is one of the novel technologies based on measurements of parameters of ultrasonic waves propagating through analyzed samples, which can be utilized for real-time non-invasive monitoring of chemical reactions. It does not require optical transparency, optical markers and is applicable for monitoring of reactions in continuous media and in micro/nano bioreactors (e.g., nanodroplets of microemulsions). The technology enables measurements of concentrations of substrates and products over the whole course of reaction, analysis of time profiles of the degree of polymerization and molar mass of polymers and oligomers, evolutions of reaction rates, evaluation of kinetic mechanisms, measurements of kinetic and equilibrium constants and reaction Gibbs energy. It also provides tools for assessments of various aspects of performance of catalysts/enzymes including inhibition effects, reversible and irreversible thermal deactivation. In addition, ultrasonic scattering effects in dispersions allow real-time monitoring of structural changes in the medium accompanying chemical reactions.

Keywords: ultrasonic spectroscopy; HR-US; ultrasonic velocity; ultrasonic attenuation; biocatalysis; enzymes; metal surface catalysis; degree of polymerization; average molar mass; microemulsions

1. Introduction

The availability of efficient methods for real-time non-destructive monitoring of catalytic transformation between reactants and products in different reaction media, from solutions to emulsion, suspensions, or gels, is an important factor in the modern development of catalysis and its applications in industrial processes [1,2]. A variety of 'electromagnetic' spectroscopic techniques such as infrared, Raman, fluorescence, and UV-Vis, can provide real-time data on concentrations of reactant and product under varying reaction conditions [1,3–7]. However, the efficiency of these techniques is dependent on the optical transparency of medium and can be affected by light scattering in dispersions. In general, these techniques have a limited dynamic (concentration) range. In addition, UV-Vis and fluorescence spectroscopies require an optical activity of the reactants or products and, in their absence, the analysis is more complicated as chromogenic and fluorogenic substrates are needed [8–10]. Therefore, discontinuous methods are widely used for the monitoring of chemical reactions, including chromatography, mass spectrometry (MS) and capillary electrophoresis [9]. These methods involve the collection of samples from a reaction mixture, and often include invasive procedures of stepwise extractions or sample pretreatments [11], which is time-consuming and costly.

This paper describes applications of an alternative to 'electromagnetic' spectroscopy-ultrasonic spectroscopy for precision real-time non-invasive monitoring of chemical reactions in solutions

and complex dispersions. Ultrasonic spectroscopy employs high-frequency (MHz range) waves of compressions and decompressions (longitudinal deformations), which probe the elastic properties of materials determined by the intermolecular interactions/forces and the microstructural organization [12–14]. The two major parameters measured in ultrasonic spectroscopy are ultrasonic attenuation, α, and ultrasonic velocity, u. Attenuation represents the exponential decay of the amplitude of the ultrasonic wave, A, of the oscillations of pressure (or longitudinal deformation) with distance travelled, z:

$$A = A_0 e^{-\alpha z} \cos[2\pi f(\frac{z}{u} - t)] \quad (1)$$

where t is time and f is the frequency of the wave. The attenuation, α, is determined by the energy losses in compressions and decompressions in ultrasonic waves. Monitoring of ultrasonic attenuation provides information on fast (relaxation time is the order of $(2\pi f)^{-1}$) dynamics of molecular processes [15] and microstructural (down to nm scale) organization of materials, including particle sizing in emulsions and suspensions (nm and μm scales), as well as characterization of aggregation, gelation, crystallization and creaming [12,16–19].

In liquids with a limited level of ultrasonic attenuation, the ultrasonic velocity is determined by the adiabatic compressibility $\beta_S = -\frac{1}{V}\left(\frac{\partial V}{\partial P}\right)_S$, where V is the volume, P is the pressure and S the entropy, and by the density, ρ, of the medium:

$$u = \frac{1}{\sqrt{\beta_S \rho}} \quad (2)$$

Compressibility, β_S, is extremely sensitive to the molecular organization and intermolecular interactions in the medium. This can be applied in analysis of a broad range of molecular processes, including catalyzed chemical reactions, if the measurements of ultrasonic velocity are performed with sufficient accuracy [2,13,20,21]. Although ultrasonic spectroscopy has been utilized for material analysis for a long time and has demonstrated various successful applications [12,14,22], the capability of this technique in analysis of chemical reactions has been restricted by a number of factors. These include limited resolution/precision in measurements of ultrasonic parameters, the requirement for large sample volumes and often complicated measuring procedures. The development of high-resolution ultrasonic spectroscopy (HR-US), based on advances in the principles of ultrasonic measurements, electronics and digital signal processing, surpass these limitations [23]. HR-US instruments (Figure 1) enable ultrasonic measurements with exceptionally high precision, down to 0.2 mm/s for ultrasonic velocity, in a broad range of sample volumes, 0.03 mL (droplet size) to several mL with a typical frequency range 1 to 20 MHz [23,24]. High precision of this technique allows for the monitoring of small changes in the concentrations of substrates and products in chemical reactions [5,8,25,26]. In addition, the geometry of HR-US ultrasonic cells is optimized for easy filling, refilling, cleaning and sterilization. They can accommodate aggressive liquids such as strong acids or volatile organic solvents, without evaporation throughout the course of measurements. HR-US measurements can be performed in a wide range of temperatures (−40 to 130 °C), at ambient or elevated pressures, in static and flow-through regimes, and in different media ranging from dilute solutions to semisolid materials [23]. The measurements can include automated precision titrations of the analyzed liquids with a titrant [27], and also programmable temperature ramps for temperature profiling [2,28]. These qualities enable the application of HR-US technique for non-destructive real-time monitoring of chemical reactions in a broad range of media and environmental conditions.

The paper reviews the underlying principles and outcomes of application of HR-US technique for real-time monitoring of chemical reactions in continuous media and in nano-bioreactors (nanodroplets) of complex dispersions such as milks, suspensions of protein nanoparticles and microemulsions. This includes precision real-time measurements of concentrations of reactants and products (reaction progress curves), time profiles of the average degree of polymerization and of molar mass of polymers and oligomers, time profiles of the reaction rates, the monitoring of structural rearrangements

(particle size) in a course of reactions, evaluation of kinetic mechanisms, measurements of kinetic and equilibrium constants of reactions and reaction Gibbs energy. It also discusses the tools provided by this ultrasonic technology for assessment of various aspects of the performance of catalysts/enzymes including inhibition effects and reversible and irreversible thermal deactivation. Although, most of the examples discussed are the reactions catalyzed by enzymes, the detection principles and the methodologies described shall be applicable for a variety of catalysts in aqueous and non-aqueous liquids.

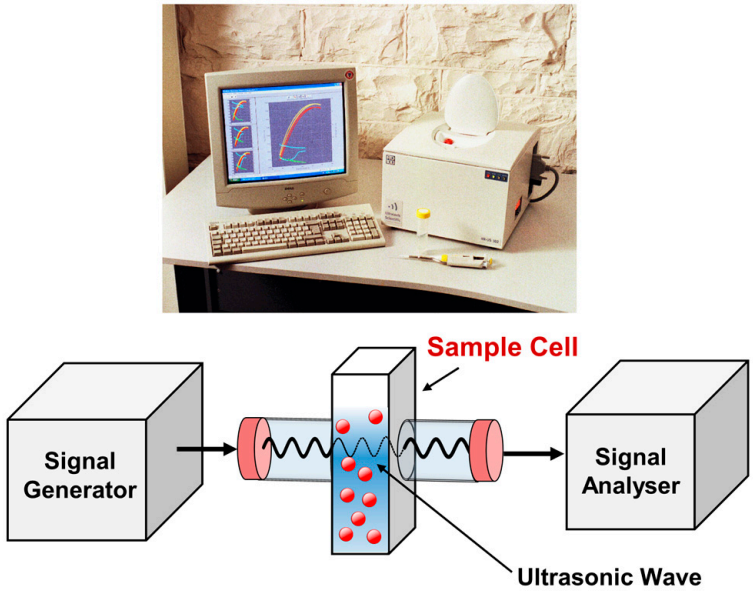

Figure 1. Illustration of operation of high-resolution ultrasonic spectrometers.

2. Monitoring of Chemical Reactions with Ultrasonic Velocity

2.1. Detection Principles. Reactions Progress Curves

Chemical reactions in a liquid mixture are accompanied by a change in the intrinsic properties of molecules involved in the reaction and by a change in their interactions with the environment, which includes solvation effects (hydration in aqueous solutions). This changes the compressibility and density of the mixture, and affects the ultrasonic velocity in the mixture. Thus, monitoring of the evolution of ultrasonic velocity, $u(t)$, with reaction time, t, shall provide real-time information on the concentration of reactants transferred to products. For a chemical reaction:

$$a_1A_1 + a_2A_2 + \ldots + a_kA_k \rightarrow b_1B_1 + b_2B_2 + \ldots + b_lB_l \quad \text{(R1)}$$

involving a_1, $a_2, \ldots, a_k$ moles of reactants A_1, $A_2, \ldots, A_k$ and producing b_1, $b_2, \ldots, b_k$ moles of products B_1, $B_2, \ldots, B_k$ the change of ultrasonic velocity within time interval δt, $\delta u(t)$, caused by the reaction can be presented as:

$$\delta u(t) = -u_0 \Delta a_r \delta c(t) \quad (3)$$

where $\delta c(t)$ is the change of concentration of one of the reactants during time interval δt and Δa_r is the concentration increment of ultrasonic velocity of the reaction defined as:

$$\Delta a_r = -\frac{1}{u_0}\frac{du}{dc} \quad (4)$$

here u_0 is the ultrasonic velocity in the reaction medium without reactants and products, and the derivative is taken at the conditions determined by Reaction (R1). The negative sign in the above

equation is introduced to compensate for the negative sign of δc over the reaction. In non-concentrated mixtures, in an absence of specific interactions between the reactants and products, the value of Δa_r is expected to be constant during the reaction, especially if the physico-chemical properties of the products are similar to the properties of the reactants. In this case the concentration $c(t)$ and the reaction extent $\zeta(t)$ can be obtained as:

$$\begin{gathered} c(t) = c^0 - \frac{u(t) - u^0}{u_0 \Delta a_r} \\ \zeta(t) = \frac{u(t) - u^0}{u_0 \Delta a_r c^0} \end{gathered} \tag{5}$$

where u^0 and c^0 are ultrasonic velocity and the concentration of the reactant in the mixture at the reaction time zero (Reaction (R1) fully shifted to the left) and $u(t)$ is ultrasonic velocity in the mixture at the reaction time t. As all concentrations of reactants and products are linked with each other by the stochiometric relationships of Reaction (R1), the concentration of any of the reactants or products or other parameter defining them (e.g., reaction extent) can be utilized in the above relationships. Although the choice of parameter representing the change of concentration of reactants and products (reaction progress) affects the concentration increment of ultrasonic velocity of the reaction, Δa_r, the value of Δa_r determined for a particular reactant or product can be recalculated into the value of Δa_r for any other reactant or product using the stochiometric relationships of Reaction (R1).

The parameter Δa_r can be presented as the difference of concentration increments of ultrasonic velocity of the reactants, a_R, and products, a_P:

$$\begin{gathered} \Delta a_r = a_P - a_R \\ a_P = \frac{u_P - u_0}{u_0 c^0};\ a_R = \frac{u_R - u_0}{u_0 c^0} \end{gathered} \tag{6}$$

here u_R and u_P are the ultrasonic velocities in the reaction mixture where the equilibrium in the analyzed reaction is shifted fully to the left ($\zeta = 0$) and to the right ($\zeta = 1$), respectively. The presence of the parameter u_0 in Equations (3)–(6) provides direct relationships linking a_R and a_P with apparent compressibility and volume of the reactants and products (see for example Reference [13]). 'Libraries' of these properties can be used for estimations of a_R, a_P and Δa_r (see Discussion in [25] as example). Although the concentration $c(t)$ can be expressed in different units, such as molarity or molality, it is useful to use moles per kg of mixture. In this case, $c(t)$ can be easily obtained from the weight fraction of the relevant component of the reaction, w, often utilized in preparations of mixtures: $c = \frac{w}{M}$, where M is the molar mass in kg/mol. If required, the molarity of a component A_i (or B_i) can be calculated from the concentration c_i (mol per kg of mixture) as:

$$[A_i] = \rho c_i \tag{7}$$

where ρ is the density of the mixture in kg/m^3. The reaction rate, r, can be obtained as a slope of the time profile of c or ζ:

$$r = -\frac{dc}{dt} = -c^0 \frac{d\zeta}{dt} \tag{8}$$

The reaction rate expressed in molarity units at time t can be obtained through multiplication of r by the density of the mixture at that time (t).

For some reactions the value of Δa_r can change in the course of the reaction due to a strong dependence of concentration increments of ultrasonic velocity of reactants and products on their concentration, or other reasons (example: decomposition of H_2O_2). For a broad range of solutions the concentration increments of ultrasonic velocity of solutes show a linear dependence on their concentration, $c(t)$. In this case, the parameter Δa_r can be presented as: $\Delta a_r = \Delta a_0 + \Delta a_1 c(t)$, where

Δa_0 and Δa_1 are constants, which do not depend on $c(t)$. In this case integration of Equation (3) with subsequent solution of the resulted quadratic equation, and selection of an appropriate solution ($c(t=0)=c^0$) provides the following relationship for calculation of $c(t)$ from ultrasonic velocity profile:

$$c(t)=\frac{\Delta a_0}{\Delta a_1}\left(\sqrt{\left(1+\frac{\Delta a_1}{\Delta a_0}c^0\right)^2-2\frac{\Delta a_1}{\Delta a_0}\frac{u(t)-u^0}{\Delta a_0 u_0}}-1\right) \quad (9)$$

At $\Delta a_1 \to 0$ this relationship is reduced to Equation (5).

2.2. Reactions Involving the Same Type of Covalent Bonds in Multiple Reactants and Products

For reactions in mixtures with multiple reactants and products involving formation or breaking of the same type of covalent bonds it is often beneficial to represent the reaction progress curves through the dependence of concentration of the bonds in the mixture as a function of time. Examples could be reactions of the hydrolysis of oligosaccharides (glycosidic bonds) and proteins (peptide bonds) discussed in subsequent chapters. The hydrolysis of these bonds can be presented as:

$$R_1-O-R_2+H_2O \to R_1-OH+HO-R_2 \quad \text{(R2)}$$

and the reaction progress can be described through the evolution of concentration of the $-O-$ bonds in the mixture. In this case, the parameter $c(t)$ in Equations (3)–(8) represents the concentration of $-O-$ bonds, hydrolysable in Reaction (R2). Consequently, the concentration increment of ultrasonic velocity of reaction, Δa_r, represents the relative change of ultrasonic velocity caused by hydrolysis of one mole of $-O-$ bonds in one kg of the mixture. Following Equation (5) the concentration of bonds hydrolyzed, $c_{bh}(t)=c^0-c(t)$, can be calculated as:

$$c_{bh}(t)=\frac{u(t)-u^0}{u_0\Delta a_r} \quad (10)$$

The parameter Δa_r is mainly determined by the difference in the hydration (solvation) level and in the intrinsic properties of the atomic groups of the reactants and of the products affected by the reaction [25]. Therefore, for sizable oligomers and for polymers the contribution of the atomic groups of reactants and products positioned outside of the local environment of $-O-$ bond to Δa_r is expected to be very small. Consequently, the value of Δa_r for hydrolysis of these molecules should not depend on the extent of hydrolysis. An exception to this are polymers with well-defined compact structure and high level of cooperativity of structural rearrangements caused by hydrolysis, affecting the hydration characteristics of their atomic groups and the intrinsic compressibility of these molecules.

The concentration of bonds hydrolyzed can be expressed in molarity units (moles of bonds hydrolyzed in one L of mixture, $[bh]$), if the density of the mixture, ρ, is known: $[bh]=\rho c_{bh}(t)$. The ultrasonically measured $[bh]$ could be employed in estimations of the change of osmolarity of solutions caused by the reaction, which is required in various applications. Another usage of the parameter $c_{bh}(t)$ is calculations of the average degree of polymerization and molar mass, discussed in the following chapter.

2.3. Degree of Polymerization and Molar Mass of Linear Polymers or Oligomers

In the case of hydrolysis of a linear polymer or oligomer, the measured concentration of bonds hydrolyzed at any time t of reaction, $c_{bh}(t)$, can be recalculated into the average degree of polymerization at this time, $\overline{DP}$, as well as into the average molar mass, $\overline{M}$ (see Appendix A.1 for

definitions). The relationships for calculations of the average degree of polymerization and of molar mass are discussed in Appendix A.1 and are the following:

$$\overline{DP} = \frac{\overline{DP}^0}{1 + c_{bh}(t)\frac{\overline{DP}^0 - 1}{{c_b}^0}}; \overline{M} = \frac{\overline{M}^0 - M_{H_2O}}{1 + c_{bh}(t)\frac{\overline{M}^0}{{w_p}^0}} + M_{H_2O} \quad (11)$$

where $\overline{DP}^0$ and $\overline{M}^0$ are consequently the average degree of polymerization and the average molar mass at time zero ($t = 0$) and ${w_p}^0$ is the weight fraction of the polymer or oligomer (kg in one kg of the mixture) at time zero, M_{H_2O} is the molar mass of water. For the concentration $c_{bh}(t)$ in Equation (11) taken in moles per kg (of mixture), the molar mass shall be expressed in kDa (kg per mole). The ratios $\frac{\overline{DP}^0 - 1}{{c_b}^0}$ and $\frac{\overline{M}^0}{{w_p}^0}$ are related to each other as: $\frac{\overline{DP}^0 - 1}{{c_b}^0} = \frac{\overline{M}^0}{{w_p}^0}$.

2.4. Calibration for Ultrasonic Velocity

Calibration of HR-US technique requires determination of the concentration increment of ultrasonic velocity of reaction, Δa_r, which allows calculations of the reaction progress curves (evolution of concentrations of reactants and products with time) from the measured time profiles of ultrasonic velocity using Equation (5), or (9), or (10). Four major methods of determination of Δa_r are outlined below.

2.4.1. Method 1

The concentration increment of ultrasonic velocity of reaction, Δa_r, can be obtained by measuring the ultrasonic velocity in the mixture containing reactants only, u_R, and velocity in the mixture containing products only, u_P, from which a_R and a_P can be obtained, and Δa_r calculated according to Equation (6). Examples of such measurements are illustrated in Figure 2A–C for hydrolysis of lactose in water and in infant milk, and for decomposition of hydrogen peroxide in water. Such measurements can be utilized for the evaluation of the dependence of Δa_r on the concentration of reactants (or products), which, however, is often small and can be neglected especially in dilute solutions.

In hydrolysis in aqueous solutions water acts as one of the reactants. Therefore, measurements of concentration increment of ultrasonic velocity of reactants, a_R, shall include water added to the reactant in an appropriate equimolar (consumed by the reaction) amount.

In this case, the contribution of reactants to ultrasonic velocity in the mixture, u_R, can be presented as a sum of the addition of other than water reactants ($R1$) to the solvent Δu_{R1} plus the effect of subsequent addition of water, Δu_w: $u_R - u_0 = \Delta u_{R1} + \Delta u_w$. Consequently, $a_R = a_{R1} + a_w$ and $\Delta a_r = (a_P - a_{R1}) - a_w$, where $a_w = \frac{\Delta u_w}{u_0 {c^0}}$. The parameter Δu_w represents the effect of dilution of the mixture with water. For non-concentrated aqueous solutions, a_w is normally small and can be neglected.

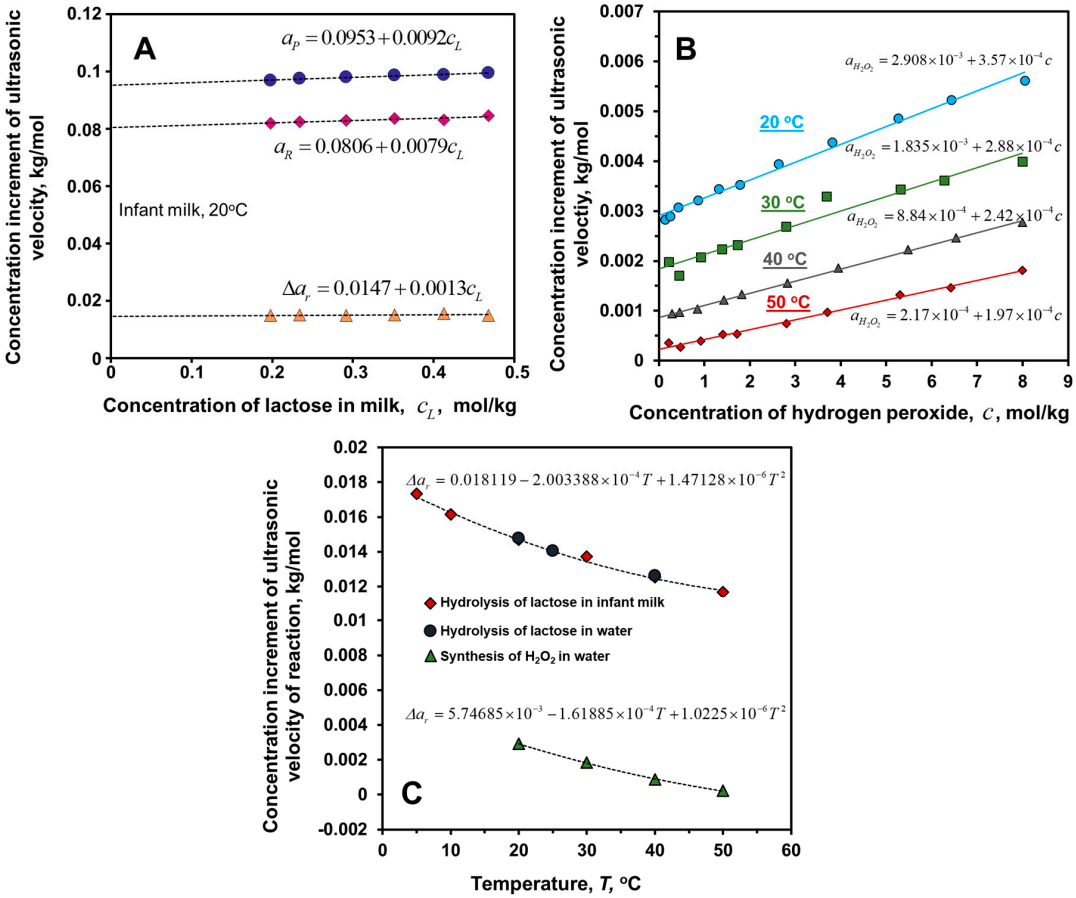

Figure 2. Application of Method 1 for measurements of concentration increments of ultrasonic velocity of reaction, Δa_r.

Figure 2A. *Hydrolysis of lactose in infant milk*.

Reaction (R4). Concentration increments of ultrasonic velocity of reactants, a_R, diamonds, (lactose, 0.198 mol/kg, plus equimolar amount of water), and products, a_P, circles, (glucose, 0.198 mol/kg, plus equimolar amount of galactose), in Cow & Gate First Infant Milk with added lactose at 20 °C at 5 MHz (no significant frequency dependence detected within 2 to 15 MHz). c_L denotes the concentration of lactose in milk prior to the addition of reactants or products. The lowest c_L (0.198 mol/kg) represents milk without added lactose. Concentration increment of ultrasonic velocity of hydrolysis, Δa_r was calculated using Equation (6). The linear dependence of Δa_r on c_L (triangles) was extrapolated to c_L = 0 to account for minor effects of lactose present in milk prior addition of reactants and products producing Δa_r = (0.0147 ± 0.0004) kg/mol [8]. Adapted with permission from Reference [8] Copyright © 2016 American Chemical Society.

Figure 2B. *Decomposition of hydrogen peroxide in water*.

Reaction (R7). The concentration increment of ultrasonic velocity of hydrogen peroxide, $a_{H_2O_2}$, in aqueous solution of different concentration, c, of H_2O_2 at 20 °C, 30 °C, 40 °C and 50 °C at 12 MHz (no significant frequency dependence detected within 2 to 12 MHz) calculated according to Equation (6). As oxygen gas produced in the decomposition of H_2O_2 is removed from the solution and the contribution of the second product, water, is negligibly small (see text) $\Delta a_r \cong -a_{H_2O_2}$. Adapted from Reference [5] with permission from The Royal Society of Chemistry. The linear fit parameters were obtained by fitting of the dependence of $a_{H_2O_2}$ on concentration of H_2O_2, which provides slightly better extrapolation of $a_{H_2O_2}$ to infinite dilution than the direct fitting of ultrasonic velocity vs. concentration utilized in [5].

Figure 2C. *Examples of temperature dependence of* Δa_r.

Red diamonds: hydrolysis of lactose in infant milk and in water [8]. Blue circles: hydrolysis of lactose in water [8]. Green triangles: decomposition of hydrogen peroxide in water at infinite dilution (calculated from plots (B)). For illustrative purposes, the negative value of concentration increment of ultrasonic velocity of decomposition of hydrogen peroxide, $-\Delta a_r$, is plotted (see Discussion in Section 6.5).

2.4.2. Method 1 in Hydrolysis of Oligomers and Polymers

For Reaction (R2) of hydrolysis of the same type of covalent bond (and same Δa_r) in a polymer and an oligomer, the concentration increment of ultrasonic velocity of the reaction (expressed through relative change of ultrasonic velocity in hydrolysis of one mole of bonds hydrolyzed in one kg of mixture) can be obtained through the measurements of ultrasonic velocity u_P in the mixture containing the products $R_1 - OH$ and $HO - R_2$ only (Reaction (R2) is fully shifted to the right) and the velocity, u_R, in the mixture containing the reactants only, (polymer or oligomer) $R_1 - O - R_2$ plus equimolar amount of water (Reaction (R2) is fully shifted to the left). The concentration c^0 in Equation (6) shall represent the concentration of the $-O-$ bonds at time zero.

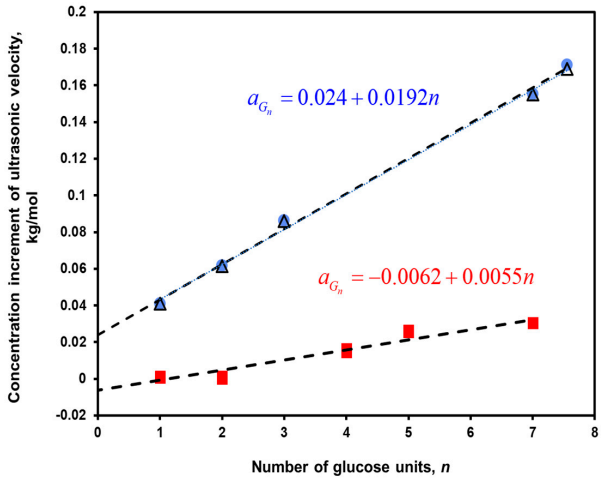

Figure 3. Concentration increments of ultrasonic velocity of maltodextrins, a_{G_n}, in aqueous solution and in isopropilmiristate microemulsion at 25 °C.
Blue circles: a_{G_n} of glucose oligomers in water at 25 °C at concentration 0.02 kg/kg calculated according to Equation (6) from ultrasonic velocities at 8 MHz (no significant frequency dependence detected within the analyzed frequency range 5 to 8 MHz).
Triangles: Same as above at concentration 0.01 kg/kg.
Red squares: a_{G_n} of glucose oligomers in the aqueous droplets of IPM microemulsion system (water (24% kg/kg), oil (isopropilmiristate (IPM), 38% kg/kg), cosurfactant (*n*-propanol, 19% kg/kg), surfactant (E200, 19% kg/kg)) at concentration 0.025 kg per kg of the aqueous phase (overall concentration 0.06 kg/kg), calculated according to Equation (6) from ultrasonic velocities at 8 MHz (no significant frequency dependence detected within the analyzed frequency range 3 to 8 MHz). Details of preparation of the microemulsion were described earlier [29–31]. n = 1—glucose, n = 2—maltose, n = 3—maltotriose, n = 4—maltotetrose, n = 5—maltopentose, n = 7—maltoheptaose, and average n = 7.55—maltodextrin (provided by manufacturer and confirmed with bicinchoninic acid (BCA) assay [32,33]).

For oligomers and polymers consisting of the same monomeric units another approach can be utilized if the concentration increments of ultrasonic velocity for homologous series are available. An example of such data for maltodextrin (oligomers of glucose) is illustrated in Figure 3. According to

the figure the concentration increment of an oligomer G_n, composed of n molecules of glucose is represented as: $a_{G_n} = b_0 + b_1 n$, where b_0 and b_1 are constants. Accordingly, the change of concentration increment of ultrasonic velocity per one bond hydrolyzed in the reaction $G_{k+l} + H_2O \rightarrow G_k + G_l$ is given as $\Delta a_r = (a_{G_k} + a_{G_l}) - (a_{G_{k+l}} + a_w)$, which produces:

$$\Delta a_r = b_0 - a_w \tag{12}$$

The parameter b_0 in this equation represents the intercept of the line drawn trough the points a_{G_n} vs. n with the Y axis at $n = 0$ (Figure 3). The results of the application of Method 1 for hydrolysis of maltodextrin in aqueous solution and in aqueous droplets of microemulsion are outlined in Table 1.

Table 1. Examples of concentration increments of ultrasonic velocity of reaction, Δa_r, kg/mol.

Reaction	Method 1	Method 2	Method 3	Conditions
Hydrolysis of lactose, Reactions (R2, R4)	$\cong 0.018119$ $-2.003388 \times 10^{-4}\ T$ $+1.47128 \times 10^{-6}\ T^2$	-	-	Infant milk, temperature, T, 10 to 50 °C [a]
Hydrolysis of lactose, Reactions (R2, R4)	0.0144 ±0.0002	0.0136 ±0.0006	-	Dilute aqueous solutions (0 to 0.2 kg/kg), 20 °C [a]
Synthesis of ATP, Reaction (R6)	-	−0.0306 ±0.0009	−0.0310 ±0.0003	Dilute aqueous solutions, of ADP, 15 mM of phosphocreatine in 50 mM gly-gly buffer, 0.02% BSA, 5 mM Mg acetate, 25 °C, pH 7.4
Hydrolysis of maltodextrin, Reactions (R2, R3)	0.0240 ±0.0002	-	-	Dilute aqueous solutions (0.01 and 0.02 kg/kg), 25 °C
Hydrolysis of maltodextrin, Reactions (R2, R3)	−0.0093 ±0.0008	-	-	IPM microemulsion, 25 °C, 0.025 kg/kg in aqueous phase
Hydrolysis of protein, β-lactoglobulin, by α-chymotrypsin, Reactions (R2, R5)	-	0.0700 ±0.0015	-	Dilute aqueous solutions (0 to 0.01 kg/kg), 25 °C, 0.1 mol/L potassium phosphate buffer, pH 7.8
Decomposition of hydrogen peroxide, Reaction (R7)	$\cong -5.74685 \times 10^{-3}$ $+1.61885 \times 10^{-4}\ T$ $-1.0225 \times 10^{-6}\ T^2$	-	-	Infinite dilution in water (for concentrated solutions see Figure 2B), temperature, T, 20 to 50 °C
Hydrolysis of cellobiose, Reactions (R2, R8)	0.0126 ±0.0002	0.013 ±0.001	-	Dilute aqueous solutions (0 to 0.1 kg/kg), 50 °C [b]

T is temperature in Celsius; [a] Reference [8]; [b] Reference [25].

2.4.3. Method 2

An alternative way to determine Δa_r involves simultaneous measurements of the change of ultrasonic velocity during the analyzed reaction and the measurements of the concentration $c(t)$, using an appropriate discontinuous technique at different reaction times. In this case according to Equation (5) the slop of the line representing the plot of $u(t) - u^0$ vs. $c_P(t) = c^0 - c(t)$, S, provides:

$$\Delta a_r = \frac{S}{u_0} \tag{13}$$

Examples of the application of discontinuous techniques for hydrolysis of peptide bonds of β-lactoglobulin, hydrolysis of lactose and synthesis of ATP are given in Figure 4A. The figure shows an increase of ultrasonic velocity with the reaction extent for the first two reactions. The primary reason for this is the higher level of hydration of atomic groups of the products when compared with the reactants [8,25,35]. The hydration effects reduce the compressibility of the water surrounding the atomic groups of reactants and products during reactions (see for example [13,25,35]) and increase the ultrasonic velocity. The opposite effect, negative S and Δa_r is observed in the synthesis of ATP accompanied by conversion of phosphocreatine to creatine, which could be explained by the lower level of hydration of products of this reaction, when compared with the reactants.

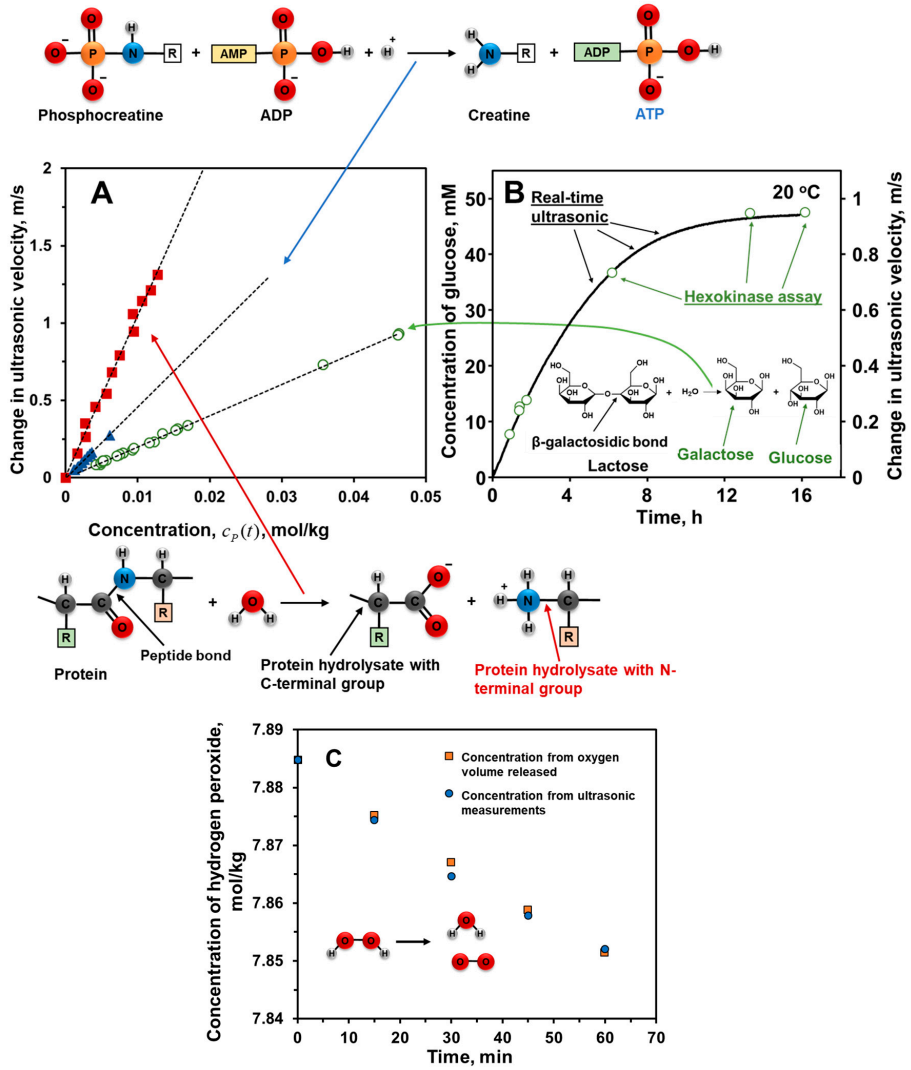

Figure 4. Application of discontinuous techniques (Method 2) for measurements or verification of Δa_r.

Figure 4A. *Change of ultrasonic velocity*, $u(t) - u^0$, *with concentration* $c_P(t)$ *in different reactions: hydrolysis of peptide bonds, hydrolysis of lactose and synthesis of ATP*.

Red squares: Reaction (R5), hydrolysis of β-lactoglobulin (0.543 mM) catalyzed by α-chymotrypsin from bovine pancreas (0.1 g/L) in 0.1 M phosphate buffer at pH 7.8, 25 °C. The ultrasonic velocity was measured at frequency 15.5 MHz. $c_P(t)$ represents the concentration of peptide bonds hydrolyzed, as determined by 2,4,6-Trinitrobenzenesulfonic acid (TNBS) method following Adler-Nissen protocol [34]. Blue triangles: Reaction (R6), synthesis of ATP (adenosine 5′-triphosphate) from ADP (adenosine 5′-diphosphate, 3.6 mM, 6.2 mM and 9.0 mM) and phosphocreatine (14.8 mM) by creatine phosphokinase from rabbit muscle (0.02 g/L) in an aqueous buffer solution (50 mM gly-gly buffer, 0.02% BSA, 5 mM Mg Acetate) at pH 7.4 and 30 °C. $c_P(t)$ represents the concentration of creatine (and ATP) formed, as determined with colorimetric hexokinase assay by monitoring the production of NADPH measured at 340 nm (hexokinase/glucose-6-phosphate dehydrogenase assay, Megazyme Int. Ltd., Bray, Ireland). For this reaction $u(t) - u^0 < 0$, however, for illustration purposes the sign of $u(t) - u^0$ was changed to positive. The ultrasonic velocity was measured at frequency 9.0 MHz.

Green circles: Reaction (R4), hydrolysis of lactose (47.9, 19, 9.83 and 5.65 mM) catalyzed by β-galactosidase (*Escherichia coli*, 369 U/g) at 20 °C in 50 mM phosphate buffer (10 mM $MgCl_2$, 10 mM mercaptoethanol) at pH 7.3. $c_P(t)$ represents the concentration of β-galactosidic bonds hydrolyzed (glucose formed) as determined with colorimetric hexokinase assay by monitoring the production of NADPH measured at 340 nm (Hexokinase/Glucose-6-phosphate dehydrogenase assay, Megazyme Int. Ltd.) [8]. The ultrasonic velocity was measured in the frequency range 2 to 16 MHz, no effect of frequency was observed.
Ultrasonic measurements were performed with HR-US 102P ultrasonic spectrometer (Sonas Technologies, Dublin, Ireland).

Figure 4B. *Comparison of ultrasonic and hexokinase assay profiles of hydrolysis of lactose by β-galactosidase in aqueous solution*.

Reaction (R4), hydrolysis of lactose (47.9 mM) by β-galactosidase (*Escherichia coli*, 369 U/g) at 20 °C in 50 mM phosphate buffer (10 mM $MgCl_2$, 10 mM mercaptoethanol) at pH 7.3. The concentration of hydrolyzed β-galactosidic bonds of lactose was calculated from the ultrasonic velocity profile (HR-US 102 ultrasonic spectrometer) using Equation (5) and Δa_r = 0.0144 kg/mol [8]. The circles represent the concentration of glucose determined with hexokinase assay in the aliquots taken from the reaction vessel at different reaction times. Frequency 5 MHz (no significant frequency dependence detected within the analyzed range 2 to 15 MHz). Adapted with permission from Reference [8]. Copyright © 2016 American Chemical Society.

Figure 4C. *Comparison of ultrasonic and volumetric (oxygen gas released) monitoring of decomposition of hydrogen peroxide in water at 25.0 °C catalyzed by an iron surface*.

Reaction (R7). Frequency 2 to 12 MHz, HR-US 102SS ultrasonic spectrometer. The samples were taken at different reaction time from the reaction vessel connected to a Hempel gas burette. No significant frequency dependence was detected within the analyzed frequency range. The ultrasonic velocity was converted to the concentration of hydrogen peroxide in the mixture using equation equivalent to Equation (9) as described earlier [5].

For reactions progressed in buffers and accompanied by a release/consumption of H^+ ions (e.g., $-NH_3{}^+ / -NH_2$ end groups of polypeptides in hydrolysis of proteins and $-OH / -O^-$ groups of phosphates in synthesis of ATP) the hydration effects of protonation/deprotonation of molecules of buffer also contribute to Δa_r. This contribution can be quantified through measuring the change of ultrasonic velocity caused by the protonation/deprotonation of buffer (acid or base titration of buffer). Such data can be used for recalculations of value of Δa_r obtained in a particular buffer into the value for another buffer.

Figure 4A shows linear dependence of the change in ultrasonic velocity in solutions of β-lactoglobulin with concentration of peptide bonds hydrolyzed. This agrees well with the kinetic mechanism of hydrolysis of globular proteins (including β-lactoglobulin) catalyzed by proteases. The hydrolysis of these proteins follows the so-called 'one-by-one' mechanism, in which the first step, demasking, represents the hydrolysis of one or several peptide bonds on protein surface that allow an enzyme to attack other bonds. Demasking is a limiting (slow) stage of the reaction. When the protein globule is 'opened' by demasking, the protein is hydrolyzed at a significantly higher rate. Therefore, polypeptides with intermediate degree of hydrolysis are nearly absent in the reaction mixture [36,37].

Figure 4B,C show good correlation between the ultrasonic reaction progress curves (parameter Δa_r obtained by Method 1) and the progress curves obtained with a discontinuous technique for hydrolysis of lactose and decomposition of hydrogen peroxide [5,8]. The results of the application of Method 2 are outlined in Table 1.

2.4.4. Method 3

For reactions with constant (over the reaction) Δa_r achieving saturation (plateau on the reaction progress curve), the value of Δa_r can be obtained from the values of $u(t) - u^0$ and $c_P(t)$ at saturation ($t = \infty$) according to the following relationship derived from Equation (5):

$$\Delta a_r = \frac{u(t=\infty) - u^0}{u_0 c_P(t=\infty)} \tag{14}$$

An example of this is the synthesis of ATP (Reaction (R6)) illustrated in Figure 8A. For the conditions at which the reaction was carried out, the equilibrium of the reaction is shifted to the products [38]. Therefore, at saturation $c_P(t = \infty)$ represents the known concentration of the reactant (ADP) at time zero. According to Table 1 obtained by Method 3 $\Delta a_r = -0.0310 \pm 0.0003$ kg/mol for this reaction is in good agreement with the result of Method 2, $\Delta a_r = -0.0306 \pm 0.0009$ kg/mol.

2.4.5. Method 4

For dilute mixtures in the absence of specific interactions between the components of reactants and products, the parameters a_R and a_P or Δa_r can be estimated from the available databases of ultrasonic or thermodynamic characteristics of the relevant atomic groups of substrates and products (see as example discussion in [25]). This could be utilized in development of 'libraries' of concentration increments of ultrasonic velocity of different reactions.

3. Monitoring of Chemical Reactions with Ultrasonic Attenuation

Ultrasonic attenuation, α, which represents the energy losses in compressions and decompressions of medium in ultrasonic wave, contains several contributions: classical, α_{class}, scattering, α_{scatt}, and intrinsic, α_{in}. In non-concentrated mixtures with limited level of attenuation these contributions are expected to be additive:

$$\alpha = \alpha_{class} + \alpha_{in} + \alpha_{scatt} \tag{15}$$

In non-concentrated dispersions, α_{in} is an additive sum of the intrinsic attenuation in the particles and in the continuous medium weighted by their volume fractions.

The classical contribution, α_{class}, represents the energy loses in the shear 'portion' of the longitudinal deformation of the medium (reaction mixture) in the wave, α_η, and also the energy losses caused by the heat flow between the parts of ultrasonic wave of different temperature, α_{TH}:

$$\begin{aligned} &\alpha_{class} = \alpha_\eta + \alpha_{TH} \\ &\alpha_\eta = \tfrac{8\pi^2}{3}\tfrac{\eta}{\rho u^3} f^2;\ \alpha_{TH} = 2\pi^2 \tfrac{T\rho\kappa e^2}{u c_P{}^2} f^2 \end{aligned} \tag{16}$$

where η is the viscosity (Pa s), ρ is the density (kg/m^3), u is the ultrasonic velocity, $e = -\frac{1}{m}\left(\frac{\partial V}{\partial T}\right)_P$ is the specific thermal expansion (m^3/(K kg)) of the medium, V is the volume of the medium and m is its mass (kg), c_P is the specific thermal capacity (J/(K kg)), κ is the thermal conductivity (W/(m K)) of the medium and T is the temperature in the medium (K) [39]. The physical properties of the medium (viscosity, specific thermal expansion, specific thermal capacity and the thermal conductivity) in the above relationships represent the properties corresponding to the ultrasonic frequencies (MHz frequency range), which sometimes may be different to those measured at low frequencies or at thermodynamic limit (zero frequency).

In non-concentrated dispersions, the intrinsic contribution to ultrasonic attenuation, α_{in}, is an additive sum of the contribution of the structural relaxation in solvent/mixture [40] and (if it exists) of the relaxation processes in fast chemical reactions. If components of the analyzed reaction are involved in a relaxation process, which time scale is comparable with the period of oscillations in the ultrasonic wave, perturbations of the equilibrium in the process caused by the oscillating pressure and

temperature in the ultrasonic wave produce a relaxation contribution to the ultrasonic attenuation, α_{rel}, and to the ultrasonic velocity, u_{rel}. For a relaxation process described by Reaction (R1) and characterized by the relaxation time τ, or by the relaxation frequency $f_{rel} = \frac{1}{2\pi\tau}$, the contribution to attenuation caused by this process in dilute solutions is given by Equations (A11) and (A12) of Appendix A.2. According to these equations the dependencies of the relaxation contributions $\frac{\alpha_{rel}}{f^2}$ and u_{rel} on the frequency have an S-shape profile with plateaus at low ($f \ll f_{rel}$) and high ($f \gg f_{rel}$) frequencies and half transition point at $f = f_{rel}$. At frequencies close to f_{rel}, the absolute value of both contributions decreases with frequency and vanishes at frequencies far above f_{rel}. At these high frequencies, the relaxation process is 'frozen' as its relaxation time is much longer than the period of oscillations of pressure and temperature in the ultrasonic wave. Measurements of the contribution of relaxation processes to ultrasonic parameters, especially to attenuation, provide additional tools for the monitoring of the chemical reaction.

The scattering contribution, α_{scatt}, is originated by non-homogeneity of the medium. It is discussed Appendix A.3. For particles of micron and submicron size at frequencies below 100 MHz (i.e., the wavelength of ultrasound is much longer than the particle radius), the incident ultrasonic wave is 'scattered' into the thermal and the viscous waves, originated at the border between the particle and the continuous medium. The thermal wave is produced by the oscillations of temperature gradient between the particle and the surrounding continuous medium, and the shear wave by the relative oscillatory motion of particles and of the continuous medium. In this case the ultrasonic velocity, u, and the ultrasonic attenuation, α, in a mixture consisting of the continuous medium (1) and the particles (2) of radius r can be obtained as the real (Re) and imaginary (Im) parts of the complex propagation constant K of the mixture outlined by Equation (A13) of Appendix A.3. The classical and intrinsic contributions to ultrasonic attenuation and velocity are included in the parameters α_1, α_2, u_1 and u_2 of this equation. According to Equations, for dispersions of solid particles of micron and submicron size, the dependence of the scattering contributions α_{scatt} measured at ultrasonic frequencies on the size of the particle has a 'bell' shape profile. The 'bell' has two, normally unresolved, maxima at the particle sizes close to (comparable with) the wavelength of the shear wave in the continuous medium and with the wavelength of the thermal wave in the particle and in the continuous medium (examples of the profiles are given in references [29,31,41]). The scattering contribution to ultrasonic velocity produces an increase of velocity with size following the S-shape profile with plateaus at small and large sizes and the transition sizes around the maxima of ultrasonic attenuation. Equations (A13) can be used in calculations of particle size in dispersions and its change during the analyzed chemical reactions.

4. Measuring Procedures

The commercially available HR-US spectrometers are comprised of at least two identical 'fill-in' or 'flow-through' ultrasonic cells (sample compartments), which volume ranges from 0.03 to several mL. Precision measurements of reaction progress often require the differential measuring regime of HR-US spectrometers. In this case, one of the cells is used as a measuring cell and the second as a reference cell. The ultrasonic parameters of media in both cells are monitored simultaneously during the reaction analysis. The measuring cell is filled with a medium close in composition to the reaction mixture. For example, for precision profiling of enzyme reactions in milks, milk can be used as a reference liquid, while for reactions carried out in non-concentrated aqueous solutions water can be placed in the reference cell. The measuring procedures are outlined below.

4.1. Procedure 1

Ultrasonic monitoring of the progress of analyzed reactions is carried out directly in the ultrasonic cells of HR-US spectrometers. The cells are preset to a required temperature using embedded temperature controller. The measuring cell is filled with the solution/dispersion containing the reactant and the reference cell (if differential regime is required) with an appropriate medium. The measurements of ultrasonic parameters are initiated, and the catalyst/enzyme is added to

the measuring cell. The mixture is stirred using an embedded or externally controlled stirrer. The measurements of the ultrasonic velocity and attenuation are constantly performed during the reaction.

4.2. Procedure 2

The reference cell (if differential regime is required) is filled with an appropriate medium. The reaction is activated in a container by mixing of the reactants and catalyst/enzyme. The mixture is placed in the measuring ultrasonic measuring cell preset to a required temperature and the measurements are performed as in Method 1. A disadvantage of this method is the time interval (up to several minutes) required for thermal equilibration in the sample placed in the measuring cell, during which the evolution of ultrasonic velocity is affected by the changing temperature. This time interval can be shortened by bringing the temperature of reactants, catalyst and the mixing container to the temperature of the ultrasonic cell prior the mixing.

4.3. Procedure 3. Measurements in Flow

The measuring flow-through cell of the HR-US spectrometer and the external reaction container (reactor) are connected with tubing. The reference cell (if differential regime is required) is filled with an appropriate medium. The reaction is activated in the reactor and the reaction mixture is constantly pumped through the ultrasonic cell and returns back to the reactor. The ultrasonic measurements are performed in flow. The volume of the commercially available flow-through cells ranges from 0.03 to several mL.

HR-US spectrometers allow simultaneous monitoring of chemical reactions at several frequencies [23]. Although the ultrasonic velocity profiles for a significant number of reactions in solutions do not depend on frequency, this is not always the case, especially if the reactants or products are involved in a relaxation process contributing to ultrasonic velocity (see Section 3). A representative example is the hydrolysis of proteins in phosphate buffer outlined below. In this case the multifrequency measurements allowed evaluation of the effects of frequency on the measured evolution of ultrasonic velocity during the reaction, as well as provided additional information on the reaction mechanism. The scattering contributions to ultrasonic parameters as well as reactions accompanied by the formation of gel could also produce a dependence of ultrasonic velocity on frequency, which can be quantified using multifrequency measurements. In addition to this, the ultrasonic particle sizing normally requires measurements of the attenuation at several frequencies. Also, the multifrequency measurements can be utilized for assessments of the formations of non-homogeneities during catalyzed reactions, caused by phase separation, aggregation, etc., which have a pronounced effect on the profiles of velocity and attenuation measured at different frequencies.

5. Add-On Capabilities

HR-US spectrometers are equipped with precision temperature controllers, which can be utilized for the monitoring of reactions during preprogramed temperature profiles. This can be applied for assessment of the effects of temperature and various temperature profiles on the reaction progress. In this case the reaction in the ultrasonic cell is started (Procedure 1 or Procedure 2) simultaneously with the activation of the desired temperature profile during which the ultrasonic velocity and attenuation are monitored in real time.

Another useful capability includes the application of titration accessories for changing the concentration of reactants, or catalysts/enzyme, or reaction inhibitors during the reaction. In this case the reaction in the ultrasonic cell is started simultaneously with the activation of the desired concentration (titration) profile during which the ultrasonic velocity and attenuation are monitored in real time. If required, the contribution of the titrant to ultrasonic parameters can be measured separately and subtracted from the reaction curves.

6. Examples of Ultrasonic Reaction Progress Curves

This chapter discusses examples of the application of the outlined methodology of ultrasonic real-time monitoring of the evolution of concentrations of reactants and products in various reactions (reaction progress curves). The majority of the reactions were catalyzed by enzymes, however, catalysis by metal surfaces is also illustrated. The discussed reactions were carried out in aqueous solutions, in the continuous phase of complex dispersions (milks) and in nano bioreactors (nanodroplets of water in w/o microemulsion).

6.1. Hydrolysis of Maltodextrin

Figure 5 shows the real-time ultrasonic profile of hydrolysis of maltodextrin, a mixture of linear saccharides, G_n, composed mainly of 7 and 8 glucose units with average degree of polymerization 7.55 catalyzed by α-amylase (*Bacillus amyloliqu efaciens*). α-amylases are enzymes that hydrolyze the α-(1-4) linkages of such polymers as starch, amylose, amylopectin, glycogen, and dextrins [42–44]. The hydrolysis can be represented as:

$$G_{k+l} + H_2O \rightarrow G_k + G_l \quad \text{(R3)}$$

where α-(1-4) glycosidic bonds ($-O-$) of G_{k+l} are hydrolyzed, producing oligomers of glucose with lower degree of polymerization, G_k and G_l.

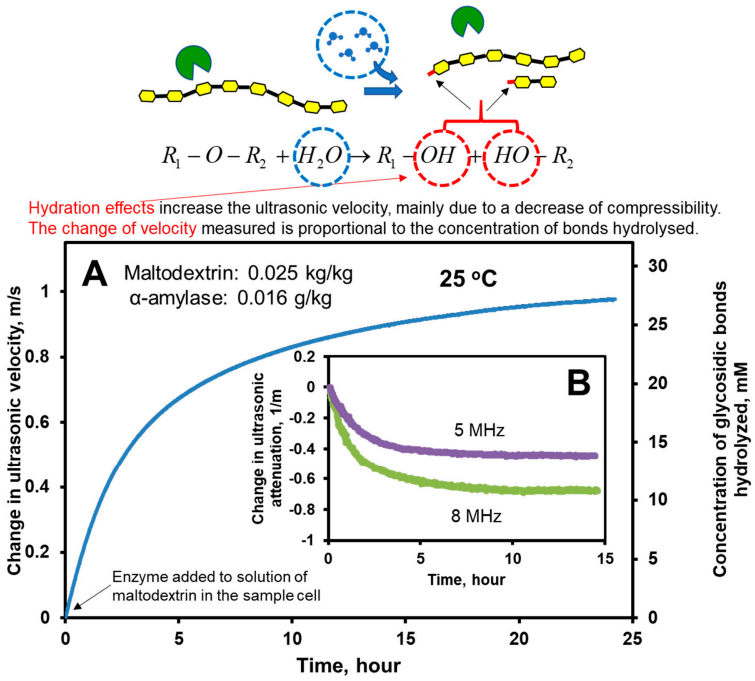

Figure 5. Real-time ultrasonic profile of hydrolysis of maltodextrin catalyzed by α-amylase. Monitoring of Reaction (R3) of hydrolysis of maltodextrin (average degree of polymerization 7.55) catalyzed by α-amylase from Bacillus sp. in 10 mM phosphate buffer at pH 6.94 at 25 °C.

Figure 5A. *Concentration profile of α-glycosidic bonds hydrolyzed.*

Calculated from the measured increase of ultrasonic velocity (HR-US 102SS spectrometer) using Equation (10) and the concentration increment of ultrasonic velocity of hydrolysis $\Delta a_r = 0.024$ kg/mol, determined by Method 1 as shown in Figure 3. Frequency 8 MHz. No effect of frequency on velocity profile was detected in the analyzed frequency range 5 to 8 MHz.

Figure 5B. *Change in ultrasonic attenuation during hydrolysis of maltodextrin catalyzed by α-amylase.*

Frequencies 5 and 8 MHz.

The reaction was started by addition of a small amount (several μL) of concentrated solution of the enzyme to the measuring ultrasonic cell of HR-US 102SS ultrasonic spectrometer preloaded with 1.4 mL of 0.025 kg/kg of maltodextrin in 10 mM phosphate buffer at pH 6.94 at 25 °C as described by Procedure 1. The concentration of the enzyme after its addition was 0.016 g/kg. The observed change in ultrasonic velocity was recalculated into the concentration (molarity) of α-glycosidic bonds hydrolyzed by applying Equations (7) and (10) and $\Delta a_r = 0.0240$ kg/mol, determined by Method 1 (Figure 3) using Equation (12), where the term a_w was neglected. The measurements were performed at frequencies 5 and 8 MHz. The ultrasonic velocity profiles at both frequencies coincide with each other within the thickness of the line on Figure 5.

The average degree of polymerization, $\overline{DP}$, and the molar mass, $\overline{M}$, were calculated according to Equation (11) and plotted in Figure 11. The degree of polymerization and the average molar mass decrease during the reaction from 7.55 and 1.224 kDa respectively to 3.31 and 0.537 kDa at reaction time of 1000 min. It is less than half of the degree of polymerization for the unhydrolyzed maltodextrin. This level of polymerization is in good agreement with the previous results on the mechanism of hydrolysis of oligosaccharides by α-amylase from *Bacillus amyloliqu efaciens* [42–44]. They demonstrated that the α-amylase cannot hydrolyze short oligomers, such as G_5, G_4, G_3 or G_2 and the hydrolysis of oligomers with 6 units, G_6, proceeds very slowly to $G_5 + G_1$ [43], while oligomers with 8 units, G_8 are mainly degraded to $G_6 + G_2$ and $G_5 + G_3$, and oligomers with 7 units, G_7 produce $G_6 + G_1$ and $G_5 + G_2$.

Overall the results presented in Figure 5 and Figure 11 (discussed below) demonstrate the capability of the HR-US technique for precision monitoring of reaction progress in the hydrolysis of oligosaccharides, which includes the real-time profiling of the average degree of polymerization and the molar mass of these molecules.

6.2. Hydrolysis of Lactose

Figure 6 illustrates the ultrasonic profiles of hydrolysis of lactose (a milk sugar) by enzyme β-galactosidase (*Kluyveromyces lactis*) in infant milk (Cow & Gate First Infant milk, 0.198 mol/kg or 6.8% kg/kg of lactose). The hydrolysis is described as:

$$Gal - O - R_2 + H_2O \rightarrow Gal - OH + HO - R_2 \quad \text{(R4)}$$

where Gal and R_2 represent the galactose and glucose moieties, and $-O-$ represents β-galactosidic linkage. The hydrolysis catalyzed by the β-galactosidase is accompanied by the production of galacto-oligosaccharides, GOS, which are prebiotics, described as β-linked chains of galactose units usually with terminal glucose. The term GOS includes the disaccharide galactose−galactose, however, excludes lactose. The majority of GOS produced by *Kluyveromyces lactis* β-galactosidase are di and tri-saccharides [8,45]. In the case of GOS R_2 represents galactose, or glucose, or disaccharide moieties of galactose-glucose or galactose-galactose. The GOS are produced at intermediate stages of the hydrolysis and are subsequently hydrolyzed. Small amount (0.7% kg/kg) of GOS are also present in infant milk as health benefit additives. For this type of hydrolysis, with multiple reactants and intermediate products, the reaction progress can be described by the evolution the concentration of β-galactosidic bonds hydrolyzed in the mixture (left Y scale on Figure 6A,B, molarity units). This parameter represents the difference between the concentration of the linkages removed from (hydrolysis of lactose and GOS) and added to (synthesis of GOS) the mixture. The presented in Figure 6 concentration of β-galactosidic bonds hydrolyzed was calculated using Equations (7) and (10). The concentration increment of ultrasonic velocity of hydrolysis of the $-O-$ linkage, Δa_r, was measured directly in milk using Method 1 (Figure 2A,C) and verified in aqueous solution using Method 2 (hexokinase assay, Figure 4) [8]. The reaction extent (supplementary Y axis) represents the ratio of the concentration of β-galactosidic bonds in the milk hydrolyzed at time t, $c_{bh}(t)$, to the amount of bonds at time zero hydrolysable by the enzyme, ${c_b}^0$ (0.198 mol/kg of the bonds of lactose and 0.025 mol/kg

of the bonds of galactooligosaccharides). The ultrasonic measurements were collected in the frequency range 2 to 15 MHz. As no significant effects of frequency on the ultrasonic velocity profiles were observed, only the data at 5 MHz are presented. Within the limits of experimental uncertainty (1% of attenuation α) no significant changes of ultrasonic attenuation were observed during the hydrolysis, thus, indicating an absence of effects of hydrolysis on microstructural characteristics of the dispersion.

The illustrated reaction progress curves allow assessment of the impact of temperature and concentration of enzyme on performance of β-galactosidase in formulations for the reduction of levels of lactose in infant milks [8]. These formulations are added to infant's milk bottles prior to baby feeding in order to overcome the frequently observed intolerance to lactose, a serious issue in the healthy development of infants.

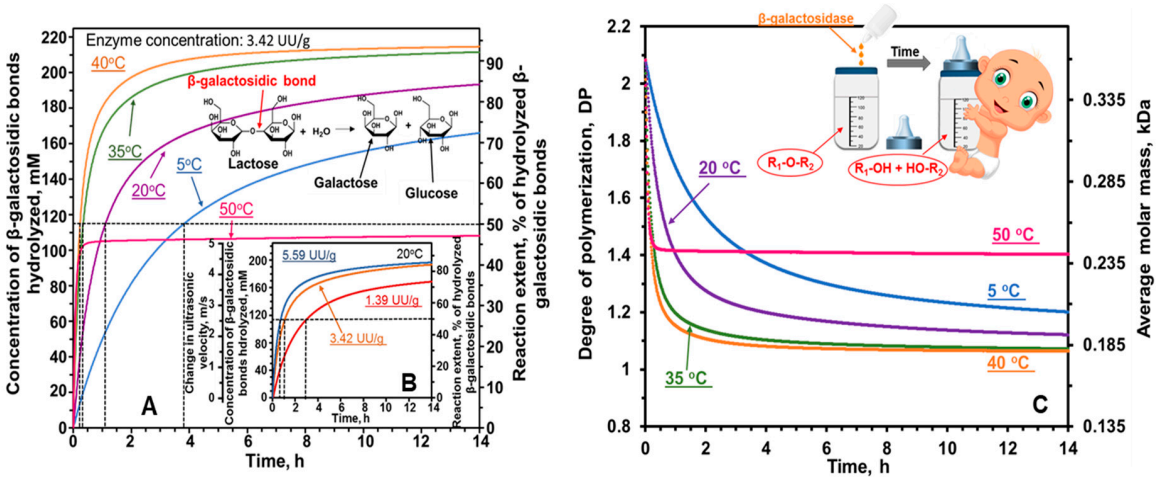

Figure 6. Real-time ultrasonic profiles of hydrolysis of lactose in infant milk by β-galactosidase.

Figure 6A. *Monitoring of Reaction (R4) of hydrolysis of lactose by enzyme in infant milk.*

β-galactosidase from Kluyveromyces lactis, Cow & Gate First Infant milk, 5 °C, 20 °C, 35 °C, 40 °C and 50 °C, enzyme concentration 3.42 UU/g.

Figure 6B. *Hydrolysis at 20 °C and enzyme concentrations 5.59, 3.42 and 1.39 UU/g.*

The concentration (molarity) profiles of β-galactosidic bonds hydrolyzed by β-galactosidase were calculated from the measured increase in ultrasonic velocity (HR-US 102PT) using Equations (7) and (10), and the concentration increment of ultrasonic velocity of hydrolysis calculated from the relationship obtained earlier [8]: $\Delta a_r(T) = 0.01812 - 2.0034 \times 10^{-4}T + 1.4713 \times 10^{-6}T^2$ kg/mol. One ultrasonic activity unit, UU, represents the amount of enzyme, which hydrolyses 1 μmol of β-galactosidic bonds in Cow & Gate First Infant milk per min at 20 °C and reaction extent equal to zero [8]. The ultrasonic measurements were collected in the frequency range 2 to 15 MHz. As no significant effects of frequency on the ultrasonic reaction profiles were observed only the data at 5 MHz are presented. Adapted with permission from Reference [8]. Copyright © 2016 American Chemical Society.

Figure 6C. *Average degree of polymerisation and molar mass of the oligosaccharides (lactose +GOS) present in the infant milk during the hydrolysis of lactose by β-galactosidase.*

Calculated from the data of Figure 6A using Equation (11). The initial degree of polymerization was obtained from UPLC-HILIC-FLD profiles of the milk published earlier [8]).

According to Figure 6A the time required for the reduction in concentration of the β-galactosidic bonds to a particular level depends significantly on the temperature of the milk. A reduction of 50% is achieved at 14 min for 40 °C and 226 min for 5 °C. At 50 °C the reaction extent levels off at 45.6% [8]. This demonstrates the fast deactivation of the enzyme at 50 °C, which is in general agreement with the results obtained for this enzyme in aqueous solutions [46]. The outlined dependence of the

enzyme activity on temperature represents one of the key challenges for practical applications of β-galactosidase in household environments.

The inset of Figure 6B shows that the time required for a particular level of hydrolysis at 20 °C is inversely proportional to enzyme concentration.

Figure 6C shows the evolution of the average degree of polymerization and the average molar mass of the oligosaccharides (lactose + GOS) present in the infant milk during hydrolysis of lactose calculated according to Equation (11). The degree of polymerization at time zero was obtained from the concentrations of lactose and added GOS (calculated from Table 1 and UPLC-HILIC-FLD profiles in Caras Altas et al. [8]) is 2.08. At temperature 40 °C and reaction time 14 h, the degree of polymerization is approximately 1.06, indicating almost fully complete hydrolysis to monomers glucose and galactose, which is in good agreement with previously obtained conclusions on the high level of hydrolysis at this temperature [45,47]. At 50 °C the degree of polymerization is approximately 1.4 at 14 h of reaction, which is explained by the fast deactivation of the enzyme at this temperature.

6.3. Hydrolysis of Proteins

Figure 7 shows real-time ultrasonic profiles of hydrolysis of globular protein β-lactoglobulin (from bovine milk) at different concentrations (0.547 and 0.273 mmol/kg) catalyzed by α-chymotrypsin in 0.1 M potassium phosphate buffer at pH 7.8 at 25 °C. The hydrolysis is described by the following reaction:

$$P_1 - C(O) - NH - P_2 + H_2O \rightarrow P_1 - COO^- + -NH_3^+ - P_2 \quad \text{(R5)}$$

where $P_1 - COO^-$ and $-NH_3^+ - P_2$ represent the protein hydrolysates with C-terminal group and protein hydrolysates with N-terminal group, respectively, and $C(O) - NH$ represents the peptide bond.

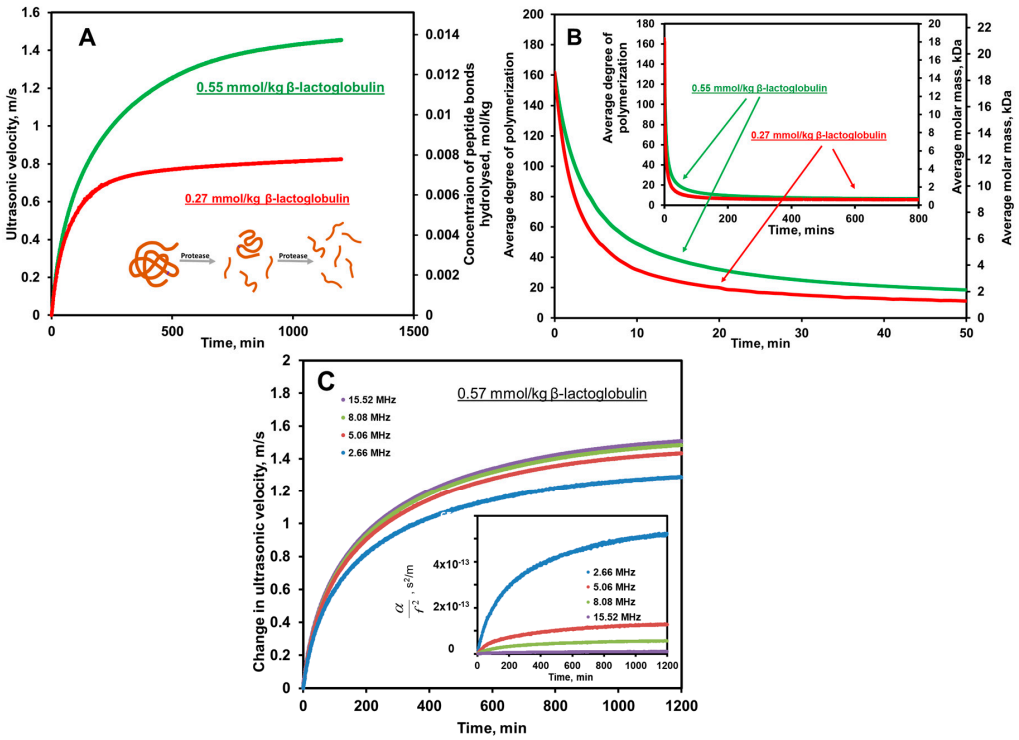

Figure 7. Real-time ultrasonic profiles of hydrolysis of protein β-lactoglobulin by proteolytic enzyme α-chymotrypsin. Reaction (R5), hydrolysis of β-lactoglobulin, in 0.1 M potassium phosphate buffer at pH 7.8 at 25 °C catalyzed by protease α-chymotrypsin from bovine pancreas 0.0021 kg/kg.

Figure 7A. *Time profiles of ultrasonic velocity at frequency 15 MHz and concentration of peptide bonds hydrolyzed.*

Concentrations of β-lactoglobulin 0.55 and 0.27 mmol/kg. The concentration of peptide bonds hydrolyzed calculated using Equation (10), and Δa_r = 0.070 kg/mol.

Figure 7B. *Real-time profiles of average degree of polymerization and molar mass.*

Calculated from the concentration of bonds hydrolyzed profile shown in Figure 7A according to Equation (11).

Figure 7C. *Time profiles for ultrasonic velocity and attenuation measured at different frequencies.*

The hydrolysis was activated by addition of several μL of concentrated solution of enzyme (α-chymotrypsin from bovine pancreas) to 1.1 mL solution of β-lactoglobulin in 0.1 M phosphate buffer at pH 7.8 preloaded into the ultrasonic cell of HR-US 102 ultrasonic spectrometer as described by Procedure 1. The concentration of enzyme in the ultrasonic cell was 0.0021 kg/kg. The ultrasonic velocity profiles were recalculated into the profiles of concentration of peptide bonds hydrolyzed, by applying Equation (10) and using Δa_r = 0.070 kg/mol determined by Method 2 (Table 1).

In contrary to the majority of reactions covered in this paper, the amplitude of the change of velocity caused by the hydrolysis of β-lactoglobulin in phosphate buffer is dependent on frequency, as illustrated by Figure 7C. The origin of this dependence is the relaxation process associated with the proton transfer between $-NH_3{}^+$ and $-NH_2$ terminal amino groups of the protein hydrolysates and the phosphate ions as discussed in the Section 9.2. According to Figure 7C, the amplitude of velocity rise becomes to be frequency independent above 10 MHz (approximately). This result agrees with the profiles of ultrasonic attenuation shown in the inset of Figure 7C (Section 9.2), thus, indicating the 'freezing' of the relaxation process (see Section 3 and Appendix A.2) at frequencies above 10 MHz. Therefore, the velocity profiles obtained at frequencies 15 MHz were used for determination of Δa_r utilizing Method 2 (Figure 4), and for the subsequent calculations of the concentration of peptide bonds hydrolyzed according to Equation (10) from the measured change in ultrasonic velocity.

Figure 7B shows the change of the average degree of polymerization, $\overline{DP}$, and the molar mass, $\overline{M}$, during the hydrolysis calculated from the concentration of peptide bonds hydrolyzed, $c_{bh}(t)$, according to Equation (11). The degree of polymerization at time zero, $\overline{DP}^0$, was taken as 162, which corresponds to the number of amino acid residues in β-lactoglobulin. Accordingly, the molar mass at time zero was taken as 18.4 kDa, which represents the molar mass of the 162 amino acids linked with the peptide bonds between them. At our experimental conditions (pH and ionic composition), β-lactoglobulin in solution is expected to exist in the forms of single molecules and the molecules aggregated into dimers [48]. Therefore, the average molar mass plotted in Figure 7B could be different to that measured with light or neutron scattering techniques or other methods, which probe the size of aggregated protein structures.

For concentration of 0.27 mmol/kg (0.005 kg/kg approx.) the average degree of polymerization, $\overline{DP}$, and the molar mass, $\overline{M}$, change from 162 and 18.4 kDa for unhydrolyzed protein to 5.5 and 0.64 kDa respectively at 1200 min. For concentration of 0.55 mmol/kg (0.01 kg/kg approx.) those values change to 6.2 and 0.70 kDa at 1200 min respectively.

The enzyme α-chymotrypsin cleaves peptide bonds selectively on the carboxyl-terminal side of the large hydrophobic aromatic amino acids such as tryptophan, tyrosine, phenylalanine, with high catalytic efficiency [49,50]. Apart from these amino acids, α-chymotrypsin also hydrolyses, although more slowly, the peptide bonds on the carboxyl-terminal side of the leucine and methionine [51,52]. Therefore, the primary structure of β-lactoglobulin allows hydrolysis by α-chymotrypsin of 36 peptide bonds of 162 amino acids present. This corresponds to the limiting value of the degree of polymerization of 4.4, which is lower, however, close to the values obtained at long reaction times.

Hydrolysis of proteins into protein hydrolysates catalyzed by proteases is utilized in a broad range of industries, from food to effective therapeutics, since the products of this reaction have additional nutritional and functional value. Enzymatic protein hydrolysates containing short-chain

peptides with characteristic amino acid composition and defined molecular size are highly desired for specific formulations, since they possess higher solubility, heat stability and valuable bioactive properties [53,54]. These hydrolysates play important roles in various aspects of health being, such as mineral binding, immunomodulatory, antioxidative, antithrombotic, hypocholesterolemic, antihypertensive function, and others [55]. Development and production of protein hydrolysates is dependent on efficient tools for real-time monitoring of the hydrolysis of peptide bonds under different environmental conditions in bioreactors. The results discussed in this chapter illustrate the potential of application of HR-US technology for this task.

6.4. Synthesis of ATP

Figure 8 illustrates ultrasonic real-time profile of synthesis ATP by the transphosphorylation of phosphocreatine to ADP catalyzed by creatine kinase at 30 °C described by reaction:

$$ADP + phosphocreatine \rightarrow ATP + creatine \quad \text{(R6)}$$

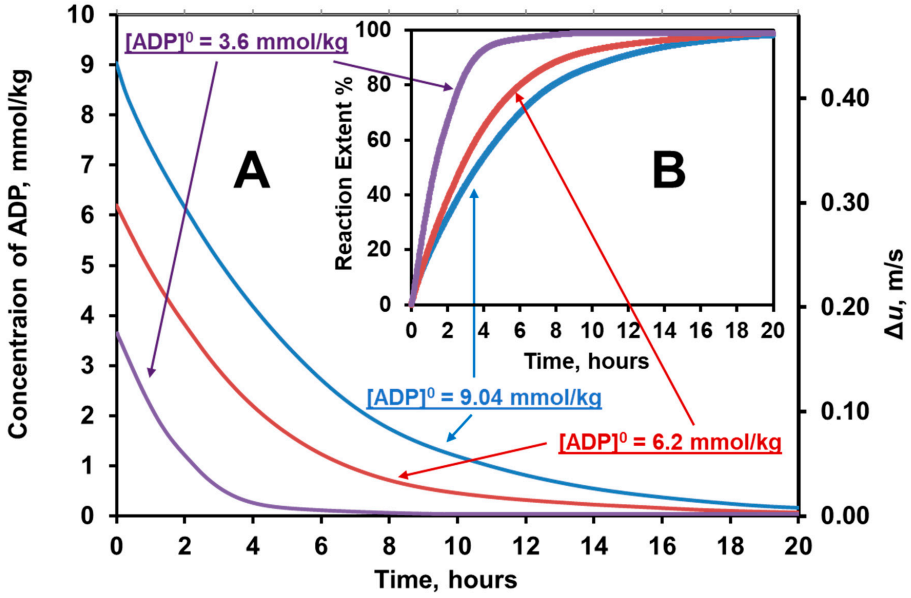

Figure 8. Real-time ultrasonic profiles of synthesis of ATP.

Figure 8A. *Ultrasonic profile of concentration of ADP during synthesis of ATP.*

Reaction (R6). Synthesis of ATP from ADP (3.6, 6.2 and 9.0 mmol/kg) accompanied by conversion of phosphocreatine to creatine by enzyme creatine phosphokinase from rabbit muscle. The reaction was performed in a buffer solution (50 mM gly-gly buffer, 0.02% BSA, 5 mM Mg Acetate at pH 7.4) at 30 °C. The concentration profile was calculated from the measured change in ultrasonic velocity at 9.0 MHz (HR-US 102 spectrometer), using Equation (5) and the concentration increment of ultrasonic velocity of hydrolysis, Δa_r = 0.031 kg/mol. For illustration purposes the decrease of ultrasonic velocity during reaction is presented as $\Delta u = u(t) - u(t = \infty)$ were $u(t = \infty)$ is the ultrasonic velocity at reaction completion.

Figure 8B. *Evolution of reaction extent in synthesis of ATP.*

Calculated from the ultrasonic velocity profile using Equation (5).

The reaction was activated by mixing of enzyme and the solutions of ADP and phosphocreatine in 50 mM gly-gly buffer, 0.02% BSA, 5 mM Mg acetate at pH 7.4 and loaded into the measuring ultrasonic cell of the HR-US 102 ultrasonic spectrometer pre-equilibrated at temperature 30 °C, following Procedure 2. The reaction was carried out at three different concentrations of ADP,

3.6 mmol/kg, 6.2 mmol/kg and 9.0 mmol/kg, and at same concentration of phosphocreatine, 15 mmol/kg. The concentration of the enzyme was 0.18 μg/mL (185 U/mg). The ultrasonic velocity profiles were recalculated into the profiles of concentration of ADP and the reaction extent by applying Equation (5) and using $\Delta a_r = -0.0310$ kg/mol determined by Method 3 and verified by Method 2 (Table 1). The concentration of ATP synthesized during the reaction at time t is equal to the difference of the initial concentration of ADP and the concentration of ADP at time t. According to Figure 8B, which represents the reaction extent, the reaction reaches completion (reaction extent = 100%) after approximately 10 h when the lowest concentration of ADP (3.6 mmol/kg) is used.

The enzyme creatine kinase occupies an important place in the regulation of muscle bioenergetics by providing rapid replenishment of the concentration of ATP from the reservoir of phosphagens [56,57]. A variety of methods have been applied for monitoring this reaction, including direct and indirect colorimetric assays. The major benefits of application of HR-US technique is the ability to monitor it precisely during the whole course of the reaction, without optical markers and/or secondary reactions, and in various media including opaque mixtures.

6.5. Decomposition of Hydrogen Peroxide Catalyzed by Metal Surfaces

Figure 9 illustrates real-time ultrasonic monitoring of the decomposition of hydrogen peroxide at 25.0 °C catalyzed by iron surface at two concentrations of hydrogen peroxide (2.81 mol/kg for the main frame and 0.0743 mol/kg for the inset) [5]. Hydrogen peroxide is used in a variety of applications, such as wastewater treatment, preparation of semiconductor materials and cleaning liquids for printed circuit boards. The decomposition of hydrogen peroxide dissolved in water can be presented as:

$$H_2O_2 \rightarrow \frac{1}{2}O_2 + H_2O \quad \text{(R7)}$$

Prior to the measurements, water was saturated with nitrogen at the measuring temperature to provide the consistency of its composition, and to prevent solubilization of CO_2 and formation of carbonic acid. After placing the aqueous solution of hydrogen peroxide into the temperature controlled reaction container (100 mL) the reaction was activated by adding the catalyst, bare iron wire (2 × 50 cm, 1 mm diameter, purity 99%+) precleaned with hydrochloric acid. The reaction vessel was connected with the measuring cell of HR-US 102SS ultrasonic spectrometer using a flexible tubing passing a peristaltic pump, as described in Procedure 3, and ultrasonic measurements were performed in flow-through regime [5]. The ultrasonic velocity profile during the reaction is given as the change of the relative ultrasonic velocity, which represents the difference between the ultrasonic velocity in the solution and in pure water. As no significant dependence of ultrasonic velocity on frequency within the frequency range 2 to 12 MHz was observed, only the data collected at 12 MHz are represented in the figure.

As the solubility of oxygen in water is very low, most of the oxygen produced in this reaction is released from the solution, with the exception of the initial stages (first minutes) when the produced oxygen substitutes nitrogen in the solution. The change in ultrasonic velocity in water caused by this substitution is at a level of 0.002 m/s and can be neglected when compared with the observed changes of ultrasonic velocity in the analyzed reaction [5]. Therefore, when considering the concentrations of reactants and products in the solution the reaction can be presented as: $H_2O_2 \rightarrow H_2O$. Consequently, the concentration increment of ultrasonic velocity of the reaction, Δa_r, can be expressed through concentration increments of ultrasonic velocity of water, a_w, and hydrogen peroxide, $a_{H_2O_2}$: $\Delta a_r = a_w - a_{H_2O_2}$. As a_w represents the effect of addition of water to water on ultrasonic velocity it is equal to zero. According to Figure 2B $a_{H_2O_2} = a_{0\ H_2O_2} + a_{1\ H_2O_2} c_{H_2O_2}$, where $a_{0\ H_2O_2}$ and $a_{1\ H_2O_2}$ are constants. Thus, for the Reaction (R7) $\Delta a_r = -a_{H_2O_2} = -a_{0\ H_2O_2} - a_{1\ H_2O_2} c_{H_2O_2}$ (see Reference [5] for details). Following this, the concentration profile of hydrogen peroxide (secondary Y axis in Figure 9) during the reaction was calculated from the ultrasonic velocity profile using Equation (9) where $\Delta a_0 = -a_{0\ H_2O_2}$ and $\Delta a_1 = -a_{1\ H_2O_2}$.

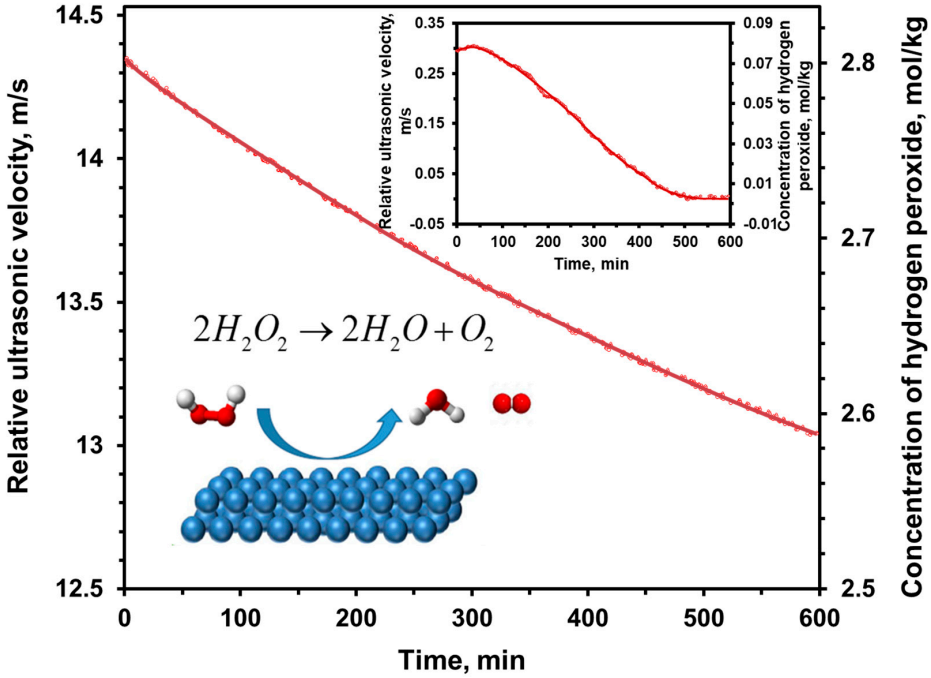

Figure 9. Real-time ultrasonic profiles of decomposition of hydrogen peroxide catalyzed by iron surface. Concentrated (2.81 mol/kg main frame) and diluted (0.0743 mol/kg, inset) aqueous solutions of hydrogen peroxide at 25 °C. The concentration profile of hydrogen peroxide was calculated from the relative ultrasonic velocity using Equation (9), and the concentration increment of ultrasonic velocity obtained earlier [5]. Adapted from Reference [5], with permission from The Royal Society of Chemistry.

At high initial concentration of hydrogen peroxide (2.81 mol/kg at time zero) the reaction rate progressively decreases with time. It is interesting to note that the time profile of the concentration of hydrogen peroxide does not correspond to the pseudo-first order reaction often applied for catalysis on surfaces [5]. This can be explained by a complex multistep nature of the reaction [58,59], which is also suggested by the ultrasonic results at the low initial concentration of hydrogen peroxide, 0.0743 mol/kg. For this concentration, an approximately 50 min delay between the introduction of the iron surface in the solution and the beginning of decomposition of hydrogen peroxide is observed. One of the possible reasons for this delay is the 'activation' of the iron surface, which could include surface oxidation (formation of Fe^{2+} ions catalyzing the decomposition [60–66]).

6.6. Encapsulation of Substrates and Enzymes. Monitoring of Reactions in Nano-Droplets

Enzymes are conventionally used in aqueous solutions. However, water is often a poor solvent for applications in synthetic and industrial chemistry [67]. Water-in-oil microemulsions (w/o ME) provide a favorable hydrophilic environment for enzyme activity [68]. In addition to this, the confined environment inside the ME droplets affects the mobility of the enzyme atomic groups and their hydration level, which can be applied for changing/controlling the enzymatic catalytical activity [67]. Examples of applications of microemulsions for enzyme catalysis of reactions include hydrolytic and reverse hydrolytic reactions, esterifications and transesterifications, resolution of racemic amino acids, oxidation and reduction of steroids, and synthesis of phenolic and aromatic amine polymers [68].

6.6.1. Microemulsion Phase Diagrams. Optimal Conditions for Encapsulation of Enzymes and Reactants

The desired functioning of enzymes encapsulated in aqueous nanodroplets is significantly determined by the level of hydration of enzyme molecules and of the molecules of substrates and products. Therefore, successful encapsulation of enzymes and of the components of reactions involves

identification of the parts of the w/o microemulsion phase diagrams where nanodroplets contain the required for the hydration of enzyme and substrate/product amount of free water. HR-US titration analysis allows for identification of these parts of microemulsion phase diagrams [31].

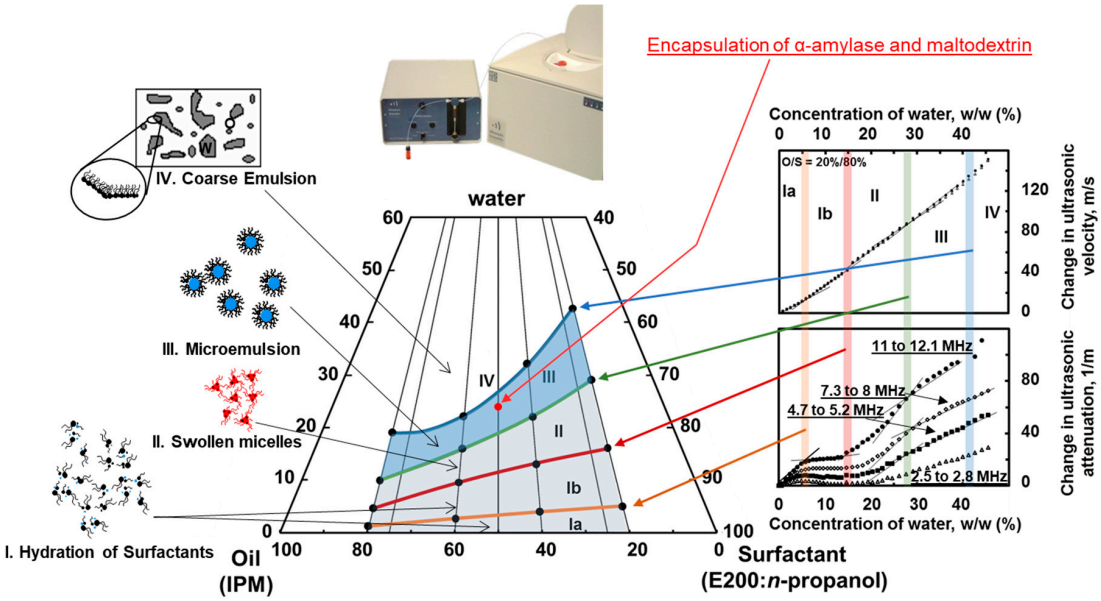

Figure 10. Ultrasonic pseudo-ternary phase diagram of IPM microemulsion.

Ultrasonic pseudo-ternary (concentration scale, % kg/kg) phase diagram of water/isopropyl myristate (IPM)/epikuron 200 (E200) and n-propanol (1:1) at 25 °C. The transition lines between different sub-phases (hydration of surfactants, swollen micelles, microemulsion and coarse emulsion) represent the 'break' points on the ultrasonic (velocity and attenuation) titration profiles of surfactant/cosurfactant and oil mixture with water. The red point shown in the phase diagram corresponds to the conditions (water (24% (kg/kg)), IPM (38% (kg/kg)), n-propanol (19% (kg/kg)), E200 (19% (kg/kg)) utilized in the hydrolysis of maltodextrin catalyzed by α-amylase in the aqueous droplets of this microemulsion system shown in Figure 11 (HR-US 102SS) ultrasonic spectrometer.

Figure 10 represents the ultrasonic phase diagram for microemulsion composed on pharmaceutically acceptable ingredients: isopropyl myristate (IPM) microemulsion (oil-IPM, surfactant-Epikuron 200 (E200)/cosurfactant-*n*-propanol (1:1), and water) at 25 °C. The diagram was obtained from titration profiles of ultrasonic velocity and attenuation, performed by automatic stepwise additions of water to 1.5 mL of a mixture of oil, surfactant and cosurfactant in the ultrasonic cell of HR-US 102SS ultrasonic spectrometer. An example of an ultrasonic titration profile in 20:80 kg/kg oil:surfactant/cosurfactant mixture is given in Figure 10. Overall, the ultrasonic titration profiles provide a number of parameters reflecting different levels of microstructural organization of the system [29,30,69]. The transitions between different states of the system are clearly identified by an abrupt change of concentration profile of ultrasonic velocity, attenuation and their frequency dependence. This includes the end of microemulsion phase represented by the blue line, above which the mixture becomes opaque (phase IV). In addition to this, the ultrasonic titration profiles demonstrate a range of transitions below the blue line, which allows distinguishing different 'sub phases', Ia, Ib, II and III. The nature of these 'sub phases' is related to the state of water and surfactant, including hydration water in the dispersed phase, hydration water in swollen reverse micelles and water in aqueous nano-size droplets surrounded by surfactant, realized in 'sub phase' III [31]. According to Figure 10 the sub-phase III shall provide a reasonable hydration level for hydrophilic enzymes, substrates and products (see more discussions in [29–31,69]).

6.6.2. HR-US Monitoring of Enzyme Catalyzed Reactions in Nanodroplets

Figure 11 compares the real-time ultrasonic profiles of hydrolysis of maltodextrin catalyzed by α-amylase from *Bacillus* sp. in aqueous solution (discussed in the Section 6.1) and in the described above w/o microemulsion consisting of oil (isoproprylmyristate, 38% kg/kg), cosurfactant (*n*-propanol, 19% kg/kg), surfactant (Epikuron 200, 19% kg/kg) and water (24% kg/kg). This composition of microemulsion was 'good' for the hydrolysis of maltodextrin, since it corresponds to the phase III of the diagram where 'free' water in macroemulsion droplets of approximately 10 nm diameter [29]. The water in the droplets shall provide a substantial hydration of the substrate (maltodextrin), of the enzyme (α-amylase) and of the products of the Reaction (R3). The concentrations of the substrate and of the enzyme in the aqueous phase of the microemulsion were close to those in the aqueous solution. The reaction in the microemulsion was started by adding of small amount (40 μL) of concentrated solution of the enzyme to the measuring ultrasonic cell of HR-US 102SS ultrasonic spectrometer preloaded with 1.4 mL of microemulsion, which aqueous phase contained 0.025 kg/kg of maltodextrin in 10 mM phosphate buffer at pH 6.94 at 25 °C according to Procedure 1.

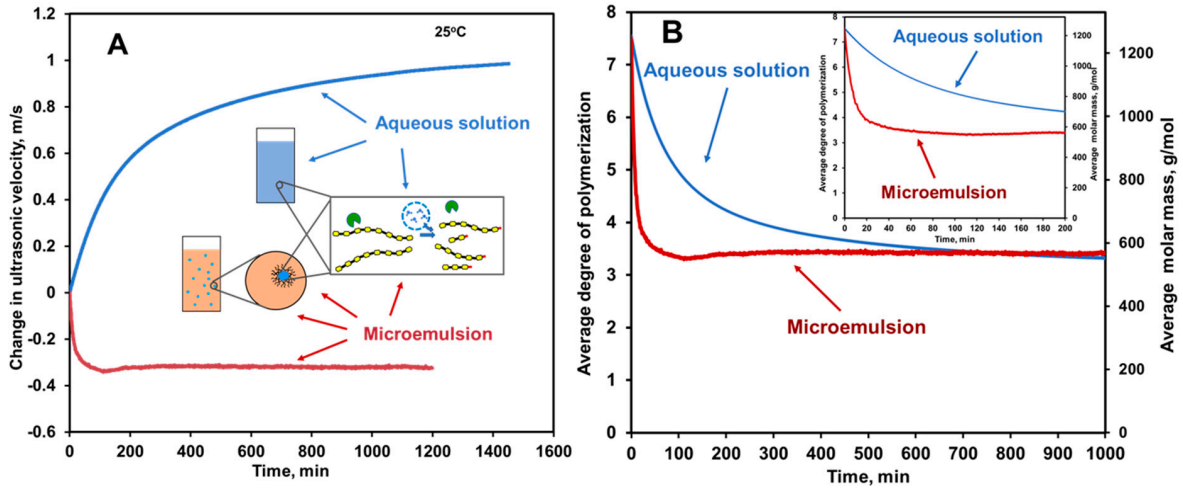

Figure 11. Real-time ultrasonic profile of hydrolysis of maltodextrin by α-amylase in aqueous solution and in nano-droplets of IPM microemulsion.

Comparison of ultrasonic profiles of hydrolysis of maltodextrin catalyzed by α-amylase (*Bacillus* sp.) in aqueous solution (conditions are outlined in the legend of Figure 5) and in microemulsion (oil (IPM, 38% kg/kg), cosurfactant (n-propanol, 19% kg/kg), surfactant (E200, 19% kg/kg) and water (24% kg/kg)).

Figure 11A. *Ultrasonic velocity profile of hydrolysis of maltodextrin catalyzed by α-amylase in aqueous solution and in microemulsion.*

Maltodextrin with concentration 0.025 kg/kg at 25 °C in 10 mM of phosphate buffer at pH 6.94. The concentrations of enzyme are 0.016 g/kg for aqueous solution and 0.015 g/kg for the aqueous phase of microemulsion system. HR-US 102SS spectrometer. Frequency 8 MHz. No effect of frequency on velocity profile was detected in the analyzed frequency range, 5 to 8 MHz for aqueous solution and 3 to 8 MHz for microemulsion. The concentrations of maltodextrin and the enzyme in microemulsion are given per kg of aqueous phase (buffer).

Figure 11B. *Real-time profiles of average degree of polymerization and of molar mass in aqueous solution and in microemulsion.*

Calculated from ultrasonic velocity profiles shown in Figure 11A according to Equation (11).

The ultrasonic velocity profiles were recalculated into the average degree of polymerization and the molar mass of oligosaccharides in the reaction mixture using Equation (11). The value of

$\Delta a_r = -0.0093$ kg/mol in the microemulsion was determined according to Method 1 and Equation (12) using the data shown in Figure 3 ($b_0 = -0.0062$ kg/mol) and the concentration increment of ultrasonic velocity of water, $a_w = 0.0031$ kg/mol measured by additions of small amounts of water to the microemulsion. For microemulsions a_w represents the slope of the plot of ultrasonic velocity vs. concentration of water illustrated in Figure 10. The negative value of Δa_r in microemulsion looks unusual, if compared with aqueous solutions. However, this can be explained by the effects of the heat exchange between the aqueous and oil phases of microemulsion during the compression cycle in the ultrasonic wave on the apparent compressibility of solutes solubilized in microemulsion nano-droplets as discussed previously [31]. The ultrasonic measurements in microemuslion were collected in the frequency range 3 to 8 MHz. As no significant effects of frequency on the ultrasonic reaction profiles were observed, only the data at 8 MHz are presented.

According to Figure 11, the reaction in microemulsion proceeds significantly faster than in solution, which could be explained by a super-activity of the enzyme, often observed in microemulsions [70–72]. This conclusion is in agreement with the previous observations of the increase in the hydrolytic activity of the α-amylase against the oligomer substrates in a presence of surfactants [42]. The average degree of polymerization and the molar mass of maltodextrin at 100 min of reaction in microemulsion are 3.3 and 0.56 kDa respectively, which is close to the values obtained in solutions at significantly longer reaction time, 1000 min, as illustrated by Figure 11B. It is interesting that in microemulsion, the decrease in ultrasonic velocity and in the degree of polymerization within 100 min of the reaction is followed by a slow increase over a longer period of time. The increase could be attributed to the previously observed alternative synthetic activities of α-amylase in restricted conditions of encapsulated state. The activities include: (1) synthesis of $-O-$ bonds between moieties of glucose (G) in maltodextrin at the initial stage of reaction forming molecules with high degree of polymerization ($G_n + G_k \rightarrow G_{n+k} + H_2O$); (2) synthesis of $-O-$ bonds between the moieties of glucose and *n*-propanol (P) present in microemulsion as cosurfactant and formation alkyl glucosides ($G_n + kP \rightarrow G_nP_k + H_2O$) [73,74].

7. Ultrasonic Reaction Rates and Advance Chemical Kinetics

High precision of ultrasonic measurements of concentration of substrates and products during analyzed reactions can be utilized in obtaining the reaction rates using Equation (8) and appropriate digital differentiation (concentration vs. time) procedures. This provides the detailed 'reaction rate vs. concentration of reactant/product' profiles over the whole course of reaction. Typically, the advanced modeling of kinetic mechanisms of chemical reaction is based on functional relationships between the reaction rate and the concentrations of reactants and products. The ultrasonic 'reaction rate vs. concentration of reactant/product' profiles can be applied for verification of these relationships and determination of the underlying kinetic and thermodynamic constants, including those involved in complex mechanisms of inhibition as illustrated below.

Figure 12 represents an example of the ultrasonic reaction rate vs. concentration of reactant profiles for hydrolysis of cellobiose (glucose disaccharide) at its different initial concentrations catalyzed by cellobiase (β-glucosidase from *Aspergillus niger* (Novozyme 188)), in 10 mM acetate buffer (pH 4.9) at 50 °C measured using Procedure 2 [25]. The overall reaction can be expressed as:

$$G_2 + H_2O \rightarrow 2G \quad \text{(R8)}$$

where G represents the molecule of glucose and G_2 the molecule of cellobiose. The 'reaction rate vs. concentration of reactant' profiles were calculated from the measured ultrasonic reaction curves ($\Delta a_r = 0.0126$ kg/mol) by averaging the slopes of two adjacent points in combination with the Savitzky–Golay smoothing method [25].

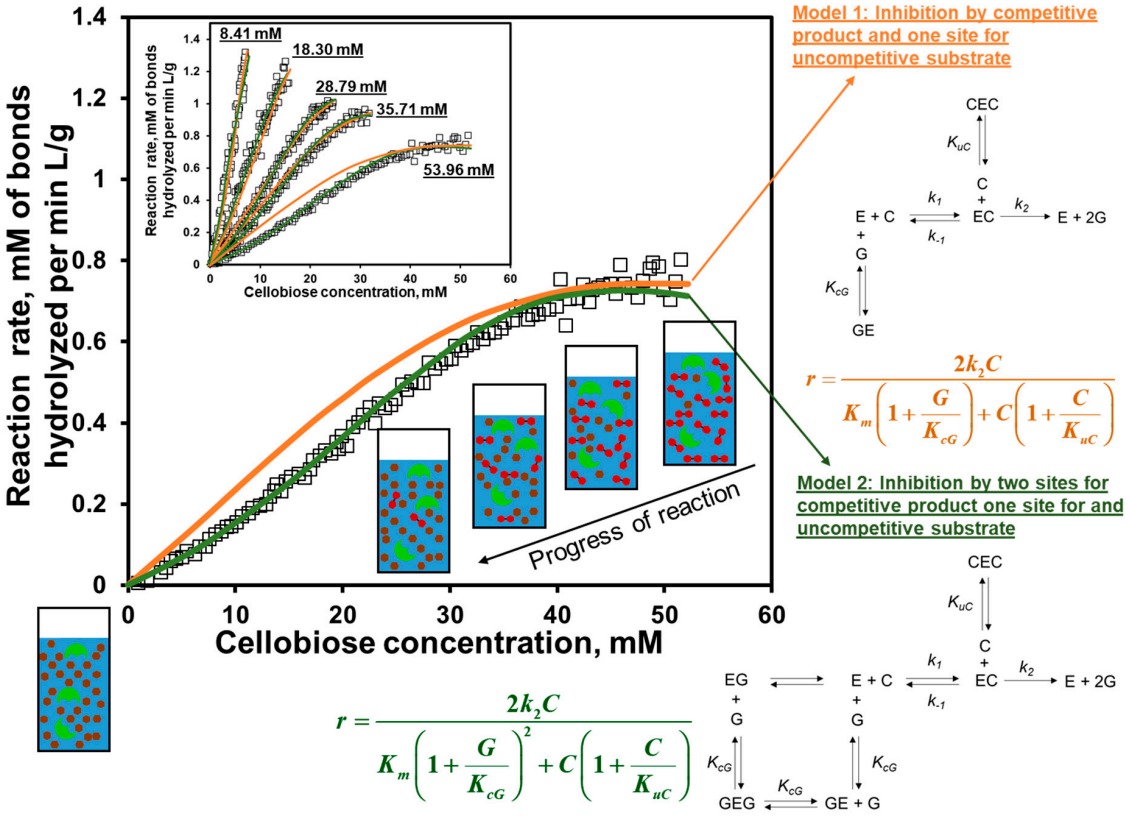

Figure 12. Ultrasonic reaction rate profile in hydrolysis of cellobiose by enzyme cellobiase. Evaluation of reaction inhibition mechanism.
Squares: Experimental reaction rates per unit of concentration (g/L) of enzyme, during hydrolysis of cellobiose, Reaction (R8).
50 °C in 10 mM acetate buffer at pH 4.9. Initial concentrations of cellobiose (curves from left to right in the inset): 8.41, 18.30, 28.79, 35.71, and 53.96 mM [25].
Lines: Fittings applied to the reaction rates for verification of two kinetic Models 1 and 2.
Orange lines: Model 1: uncompetitive substrate (cellobiose, *C*) and competitive product (glucose, *G*) inhibitions. Green lines: Model 2: uncompetitive substrate (cellobiose, *C*) and two sites for competitive product (glucose, *G*) inhibitions. Adapted with permission from Reference [25]. Copyright © 2011 Elsevier Inc.

Previous studies of kinetics of the hydrolysis of cellobiose catalyzed by β-glucosidase from *A. niger* have shown that the reaction follows uncompetitive cellobiose and competitive glucose inhibitions [25,75,76]. The proposed model of such inhibition is illustrated in Figure 12 (Model 1). According to this model, glucose binds to the free enzyme decreasing the apparent affinity of the substrate, whereas cellobiose inhibits hydrolysis by binding to the enzyme–substrate complex, thus reducing its effective concentration. The parameter $K_m = \frac{k_{-1}+k_2}{k_2}$ represents the Michaelis constant, k_1 and k_{-1} are the rate coefficients for the formation of complex EC, and k_2 is the catalytic coefficient (see Figure 12). The inhibition constants are presented by the parameters K_{cG} and K_{cG} (constants of dissociation of GE to $G + E$ and CEC to $EC + C$). The expression for the reaction rate, r, for this model [77] is given as:

$$r = \frac{2k_2C}{K_m\left(1+\frac{G}{K_{cG}}\right)+C\left(1+\frac{C}{K_{uC}}\right)} \quad (17)$$

where C is the concentration of cellobiose and G is the concentration of glucose in the reaction mixture. Figure 12 shows the ultrasonic reaction rate profiles (squares) over the course of reaction for different

initial concentrations of cellobiose (8.41, 18.30, 28.79, 35.71, and 53.96 mM) and their fitting (combined fitting of all curves) using Equation (17).

Although Model 1 describes reasonably well the profiles for low initial concentrations of cellobiose (8.41, 18.30 and 28.79), a significant deviation of this mathematical model from the experimental data can be noticed at the highest initial concentration of cellobiose (53.96 mM, main frame of Figure 12). More importantly, at a high initial concentration of cellobiose, the experimental reaction rate curve exhibits an S-shape profile that cannot be reproduced by Equation (17) [25]. Thereby, a new, updated kinetic inhibition model was proposed as illustrated in Figure 12 (Model 2). Model 2 suggests two (instead of one) binding sites for glucose on the enzyme. For simplicity, it was suggested that both sites are characterized by the same dissociation constant, K_{cG}. Additionally, it was speculated that the second site for glucose binding may be related to the known secondary, transgalactosylation, activity of the enzyme [25]. The equation for the rate representing Model 2 is given as:

$$r = \frac{2k_2C}{K_m\left(1+\frac{G}{K_{cG}}\right)^2 + C\left(1+\frac{C}{K_{uC}}\right)} \quad (18)$$

Figure 12 shows the fitting (combined fitting of all curves) of the experimental data with Equation (18) at different initial concentrations of cellobiose. This fitting describes the experimental results very well and provides the kinetic and thermodynamic constants of the reaction, k_2, K_m, K_{cG} and K_{uC} [25].

8. Application of Extended Capabilities of Ultrasonic Spectroscopy

8.1. Dynamic Range

One of the important features of HR-US technique is its capability to work with solutions of low and high concentrations (e.g., dynamic range). This includes precision monitoring of changes in small fraction of reactants presented in large concentration. Applications of this feature are illustrated by the two following examples.

8.1.1. Ultrasonic Monitoring of Reverse Reactions

Figure 13A illustrates the ultrasonic reaction progress curve of hydrolysis (Reaction (R8)) of disaccharide cellobiose consisting of two molecules of glucose catalyzed by β-glucosidase from *Aspergillus niger* in 10 mM acetate buffer at pH 4.9 at 50 °C measured using Procedure 2 [25]. The parameter Δa_r = 0.0126 kg/mol was obtained by Method 1, and verified by Method 2 (hexokinase assay).

Figure 13B illustrates the ultrasonic reaction progress curve of the reverse Reaction (R8), synthesis of cellobiose from glucose, catalyzed by the same enzyme. The synthesis was initiated by adding the enzyme β-glucosidase to the solution of glucose in 10 mM acetate buffer at pH 4.9 at 50 °C using Procedure 2 [25]. At equilibrium in Reaction (R8) the concentration of cellobiose represent only small fraction of concentration of glucose. Therefore, relatively high concentrations of glucose (0.56 mol L^{-1} for the profile presented in the Figure 13B,C) were used. The presented ultrasonic velocity profile was obtained at frequency 5.3 MHz, however, no significant effect of frequency on the profiles were observed in the analyzed frequency range 2 to 20 MHz [25]. The change in the concentrations of glucose was calculated from the ultrasonic velocity profiles using Equations (5) and (7) and the parameter Δa_r corrected for small deviation from the above value caused by high concentration of glucose [25]. As can be seen from the Figure 13C less than 3% of glucose present in the solution reacted at the saturation level. In spite of this small fraction of glucose consumed by the synthesis, the reaction profile is well resolved by the HR-US technique. The obtained saturation level provides the equilibrium concentration of glucose in the solution for Reaction (R8), which allows calculations of the equilibrium constant of the reaction, K_{eq}. The equilibrium constants K_{eq} (expressed through mole fractions of cellobiose, water and glucose) obtained in this way in solutions of different concentration of glucose

are shown in Figure 13D and correspond to the average value of 1.8 ± 0.1. The obtained equilibrium constants allowed the calculations of the standard Gibbs energy of reaction $\Delta G^0 = -8$ kJ/mol, which agrees with the results obtained by other techniques [25].

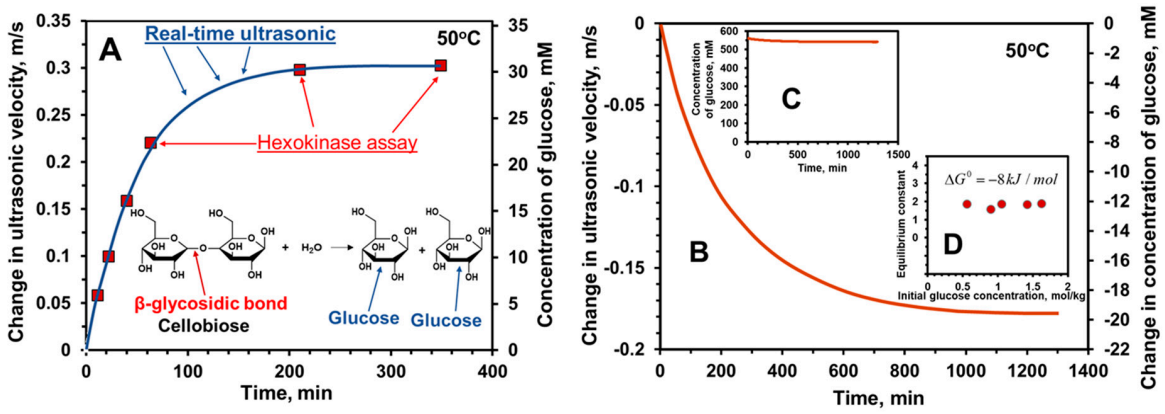

Figure 13. Real-time ultrasonic profile of hydrolysis and of reverse reaction of synthesis of cellobiose by enzyme β-glucosidase. Evaluation of reaction equilibrium constant and Gibbs energy.

Figure 13A. *Ultrasonic reaction profile of hydrolysis of cellobiose by β-glucosidase.*

Reaction (R8). 15.6 mmol/kg of cellobiose and 0.32 g/L of β-glucosidase. Squares represent the concentration of β-glycosidic bonds hydrolyzed (glucose formed) determined by colorimetric hexokinase assay by monitoring the production of NADPH measured at 340 nm (Megazyme Int. Ltd.) [8]. $\Delta a_r = 0.0126$ kg/mol was applied in calculations of the profile of concentration of glucose.

Figure 13B. *Time profile of concentration of glucose during reverse reaction (glucose condensation) catalyzed by β-glucosidase.*

20.3 g/L of β-glucosidase in aqueous solution of glucose at concentration 0.56 mol/kg, at 50 °C in 10 mM acetate buffer at pH 4.9. The change in concentration of glucose was calculated from the ultrasonic velocity profile [25].

Figure 13C. *Time profile of the overall concentration of glucose present in the reactional mixture during the reverse reaction catalyzed by β-glucosidase.*

Figure 13D. *Equilibrium constant, K_{eq}, of reaction of glucose condensation obtained at different concentrations of glucose.*

50 °C in 10 mM acetate buffer at pH 4.9. The presented ultrasonic velocity profiles were obtained at frequency 5.3 MHz with HR-US 102 ultrasonic spectrometer. No significant effect of frequency on the profiles were observed in the analyzed frequency range 2 to 20 MHz [25].
The concentrations of enzyme are given as mass (g) of Novozyme 188 liquid preparation (concentration of protein 184 mg/mL, density 1.23 g/mL at room temperature) per liter of solution.

8.1.2. Assessment of Enzyme Deactivation during Long-Time Reactions

Quantitative assessment of deactivation of enzyme during catalyzed processes is an important, however, often difficult and expensive task [78]. Figure 14 illustrates a direct ultrasonic assessment of stability of β-galactosidase in Cow & Gate First Infant milk at 20 °C during hydrolysis of lactose catalyzed by this enzyme over 24 h. The small concentration of enzyme utilized in the test was chosen to provide small (however measurable) change of concentration of the substrate (3% or 13 cm/s increase in ultrasonic velocity over 24 h), so that the hydrolysis occurred at nearly constant concentration of the substrate (as shown in the inset of Figure 14) [8]. The reaction was started by injection of a small (several μL) of diluted solution of enzyme (0.005 UU/g) to the measuring ultrasonic cell of HR-US 102 spectrometer containing 1.2 mL of infant milk, as described by Procedure 1. The concentration profile

shown in Figure 14 was calculated from the measured ultrasonic velocity by applying Equations (5) and (7). The mainframe of Figure 14 also shows the reaction profile expected in an absence of enzyme deactivation (see [8] for details).

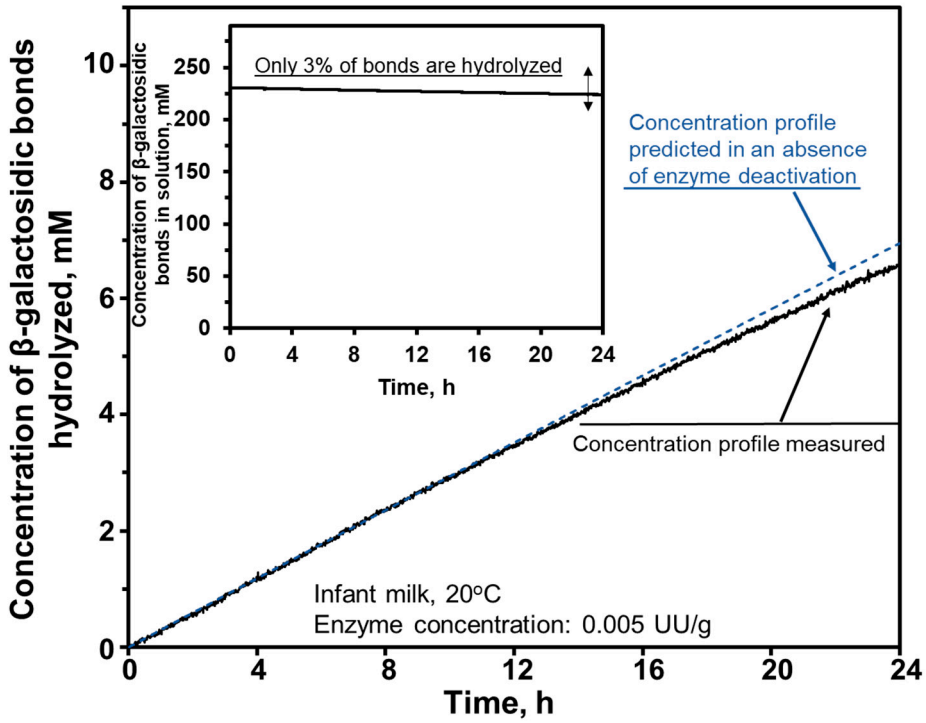

Figure 14. Ultrasonic assessment of deactivation of enzyme β-galactosidase during long time hydrolysis of lactose in milk.

Main frame. *24 h evolution of concentration of β-galactosidic bonds in Cow & Gate First Infant Milk during hydrolysis of the bonds by β-galactosidase.*

Reaction (R4). β-galactosidase from *Kluyveromyces lactis*, 0.005 UU/g, at 20 °C. The concentration (molarity) profile was calculated from the monitored change of ultrasonic velocity using Equations (7) and (10) and Δa_r = 0.0147 kg/mol. The black line represents the measured (HR-US 102 spectrometer) profile. The blue line represents the reaction profile expected in an absence of enzyme deactivation (see [8] for details).

Inset. *Total concentration of β-galactosidic bonds present in the reactional mixture during hydrolysis in Cow & Gate First Infant Milk.*

Calculated from the same as in the main frame ultrasonic profile according to Equation (5), where c^0 represent the concentration of β-galactosidic bonds of lactose and GOS in milk.
The ultrasonic measurements were collected in the frequency range 2 to 15 MHz. As no significant effects of frequency on the ultrasonic reaction profiles were observed, only the data at 5 MHz are presented. Adapted with permission from Reference [8]. Copyright © 2016 American Chemical Society.

According to the figure, at times above 16 h the reaction profile deviates from the one predicted in an absence of enzyme deactivation, which could be interpreted as a beginning of progressive enzyme deactivation.

8.2. Titrations in Analysis of Effects of Enzyme Concentration

The effect of concentration of enzyme on its activity is an important factor in the design of enzyme based formulations. It is commonly assessed by measuring the initial reaction rates in a set of samples containing enzyme of different concentrations. Figure 15 illustrates an alternative methodology

for the assessment of the effects of concentration of enzyme β-galactosidase on its activity in milk. The methodology utilizes titration capabilities of HR-US technique. The measurements were performed by titrating the infant milk in the ultrasonic cell with concentrated solution of β-galactosidase at 20 °C using pre-programmed precision injections by HR-US 102 titration accessory. Each injection was followed by a short period of stirring and a period without stirring. The mainframe of the figure represents ultrasonic velocity profiles (secondary Y axis) during time intervals between the stirring periods and subsequent injections. The circles on the inset in Figure 15 represent the initial rates of hydrolysis, r^0, calculated from the slopes of linear parts of the dependences at each step of the titration (see [8] for details). According to the figure, the initial reaction rate, r^0, increases linearly with concentration of the enzyme, thus, indicating that the specific activity of the β-galactosidase in the milk does not depend on its concentration within the analyzed concentration range.

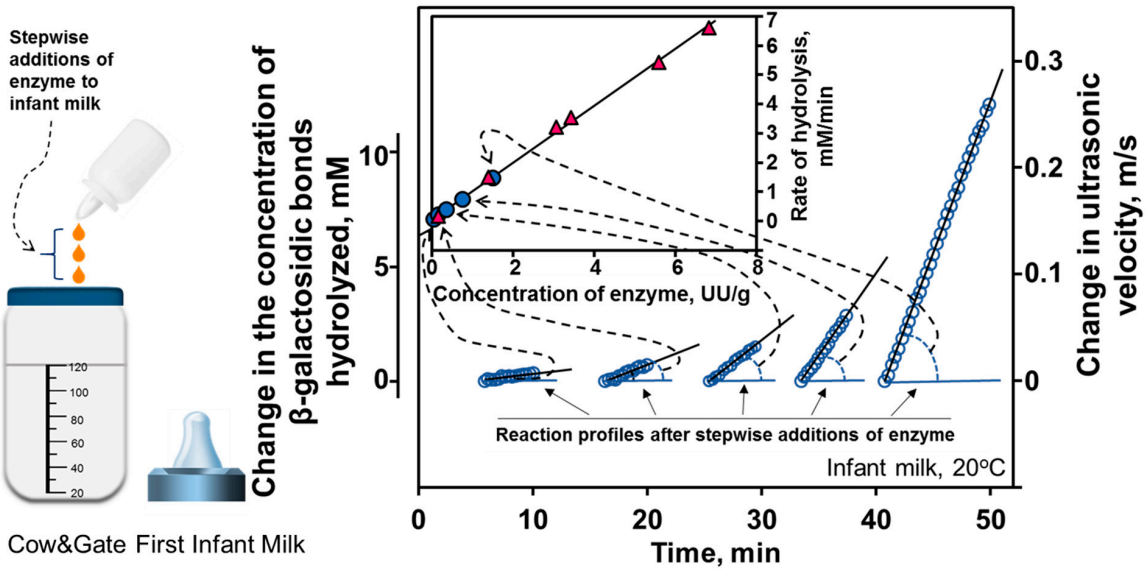

Figure 15. Ultrasonic assessment of effects of enzyme (β-galactosidase) concentration on its activity in hydrolysis of lactose in milk.

Main frame. *Time profiles of ultrasonic velocity in Cow & Gate First Infant Milk after automatic stepwise additions of β-galactosidase (Kluyveromyces lactis) at 20 °C.*

The change in the concentration (molarity) of β-galactosidic bonds (lactose and GOS, Reaction (R4)) hydrolyzed was calculated from the measured increase in ultrasonic velocity (HR-US102PT spectrometer) according to Equations (10) and Δa_r = 0.0147 kg/mol.

Inset. *The initial rates of hydrolysis.*

The circles represent the initial rates of hydrolysis, obtained from the slopes shown in the mainframe corrected for 'inhibition' effects [8]. Triangles represent the initial reaction rates obtained from separately measured ultrasonic progress curves as those shown in Figure 6B.
The ultrasonic measurements were collected in the frequency range 2 to 15 MHz. As no significant effects of frequency on the ultrasonic reaction profiles were observed, only the data at 5 MHz are presented. Adapted with permission from Reference [8]. Copyright © 2016 American Chemical Society.

8.3. Temperature Profiling

Reversible and irreversible effects of temperature on activity of enzymes is one of the key properties determining the enzymes applicability. They are commonly assessed by measuring the initial reaction rates in a set of samples at different temperatures. Figure 16 illustrates an alternative methodology, based on the measurements in a single sample utilizing the programmed temperature profiling capabilities of HR-US technique for the enzyme β-galactosidase (Reaction (R4)) in milk [8].

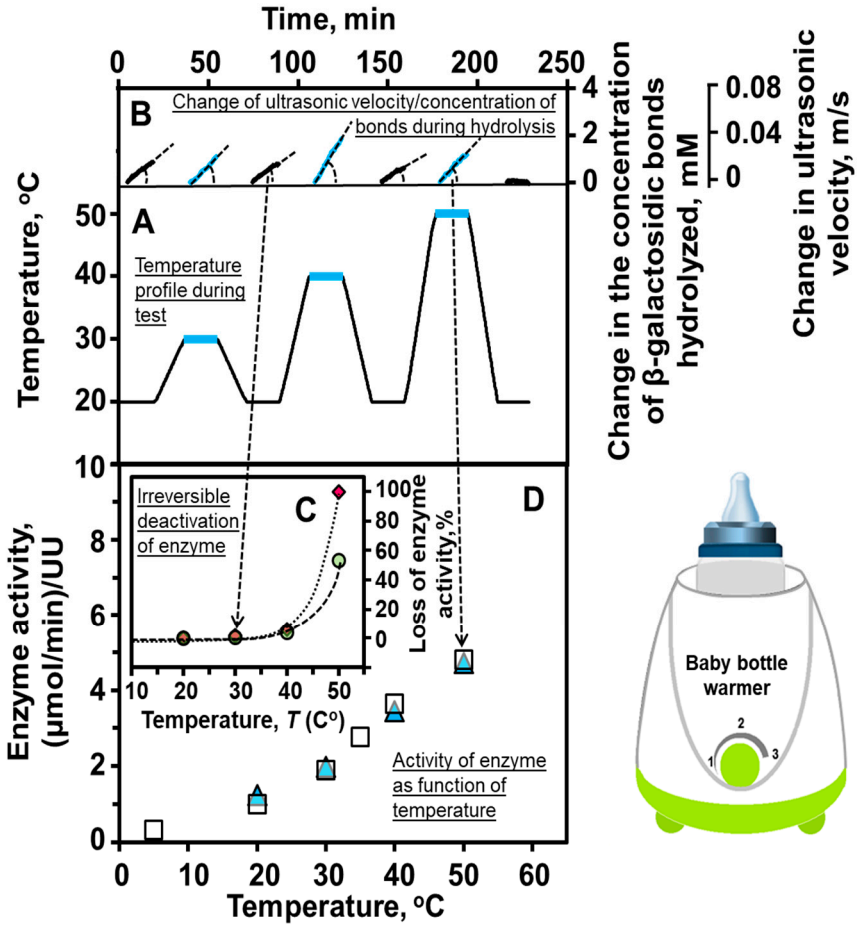

Figure 16. Ultrasonic assessment of reversible and non-reversible effects of temperature on activity of β-galactosidase in milk.

Effect of temperature on the rate of hydrolysis of β-galactosidic bonds (lactose and GOS, Reaction (R4)) in Cow & Gate First Infant Milk catalyzed by β-galactosidase (concentration 0.042 UU/g), reversible and irreversible deactivation of enzyme.

Figure 16A. *Temperature of the milk in ultrasonic cell in during single sample programmed temperature profiling.*

Figure 16B. *Ultrasonic velocity profiles at time intervals of constant temperature.*

HR-US-102PT ultrasonic spectrometer.

Figure 16C. *Irreversible loss of enzyme activity with temperature.*

Diamonds: The fractions of deactivated enzyme measured at subsequent (to the indicated temperatures) 20 °C time intervals, and presented as % of activity at the precluding 20 °C interval. Circles. The fractions of deactivated enzyme at each elevated temperature, calculated as the average of the fractions for the precluding and the subsequent 20 °C interval.

Figure 16D. *Effect of temperature on activity of active enzyme.*

Triangles: Calculated from the slopes ultrasonic velocity vs. time (B). Squares: the enzyme activities obtained from separately measured reaction profiles (Figure 2) [6]. Adapted with permission from Reference [8]. Copyright © 2016 American Chemical Society.

The measuring and the reference cells of HR-US 102 spectrometer were filled with 1.1 mL of infant milk. After equilibration at temperature 20 °C, 2 μL of β-galactosidase from Kluyveromyces lactis (aqueous solution, 21.6 UU/g, see figure legend for details) was added to the ultrasonic measuring cell, using Procedure 1. After the stirring of the sample using a mechanical mini stirrer for 30 s, the

temperature profile (20 min time intervals at 20–30–20–40–20–50–20 °C, Figure 16A) was activated. The measured 'ultrasonic velocity vs. time profiles' (Figure 16B) provided the concentration of β-galactosidic bonds hydrolyzed, and the reaction rates r^0, calculated from the slopes ultrasonic velocity vs. time using Equations (8) and (10) with correction for inhibition effects (see [8] for details). The diamonds on Figure 16C illustrate the fraction of non-reversibly deactivated enzyme caused by heating from 20 °C to a particular temperature and subsequent cooling to 20 °C measured as a reduction of r^0 at 20 °C. The circles represent the fractions of deactivated enzyme at each elevated temperature, estimated as the average of the fractions for the precluding and the subsequent 20 °C interval. Figure 16D represents the level of activity of active enzyme at each elevated temperature interval calculated as a ratio of r^0 to the concentration of active enzyme expressed with ultrasonic activity units, UU (see Figure 6 legend for UU definition). The enzyme activities obtained from separately measured reaction profiles (e.g., Figure 6A) were added to the figure as opened squares. The highest specific activity was observed at 50 °C, which exceeds by approximately 2.5 times the activity at 30 °C. This agrees with previous results in buffers for chromogenic substrate ONPG [79]. Figure 16 shows that an exposure of the reaction mixture to temperature of 40 °C and above causes progressive irreversible deactivation of enzyme, which is particularly fast at 50 °C. The ultrasonic attenuation, measured during the test, has decreased with temperature, however, recovered to the original values at each 20 °C interval, thus, indicating an absence of irreversible effects of temperature on the milk microstructure during the test. The illustrated results allow optimization of the efficiency of commercial enzyme formulations for lactose-intolerant infants (see [8] for details).

9. Monitoring of Ultrasonic Attenuation

9.1. Structural Rearrangements and Particle Sizing

Figure 17 represents real-time ultrasonic monitoring of enzymatic removal of the 'hairy' layer of hydrated protein nanoparticles (casein micelles, 120 nm diameter approx.), followed by particle aggregation and gelation in milk at 30 °C [80]. The κ-casein 'hairy' layer provides steric stability of the particle dispersion. Its enzymatic removal leads to particle aggregation and formation of particle gel, which is utilized in cheese making (renneting process).

The measurements were performed according to Procedure 2 using HR-US 102 ultrasonic spectrometer in multifrequency regime in which the data measured at several pre-selected frequencies between 2 and 15 MHz were collected simultaneously. The enzyme (rennet, chymosin) was added to milk reconstituted from skim milk powder. The volume fraction of micelles, composed of casein and water, was 0.1. The ultrasonic attenuation profiles for different frequencies are presented in the inset and the profile for frequency 14.5 MHz is plotted in the main frame. This profile was recalculated into the evolution of the 'average' (over ultrasonic scattering profile, attenuation vs. size, see examples of the profiles in [30,41,81]) size of the protein particles during the process using the particle sizing module of HRUS 102 software, which utilized the equations as those discussed in Appendix A.3. The volume fraction of casein micelles was assumed to be constant. The physical parameters of the casein micelles and of the continuous medium utilized in these calculations were taken from data published by Griffin et al. [82]. Minor amendments of some parameters were introduced to account for small differences in temperature to which the parameters were originally attributed and the temperature at which the measurements were performed [80].

The particle size scale is presented on the right Y axis of the figure. According to the figure the average size of the particles decreases within first 8 min of reaction. The decrease in diameter from the initial size (120 nm [83]) is approximately 20 nm, which corresponds to the expected size of the particle 'hairy' layer [83]. This is followed by the increase of the size, which demonstrated the beginning of the aggregation of 'bald' particles. At the reaction time 30 min, further aggregation of particles results in a formation of gel network, as indicated by rheological (rise of shear storage modulus) data [80].

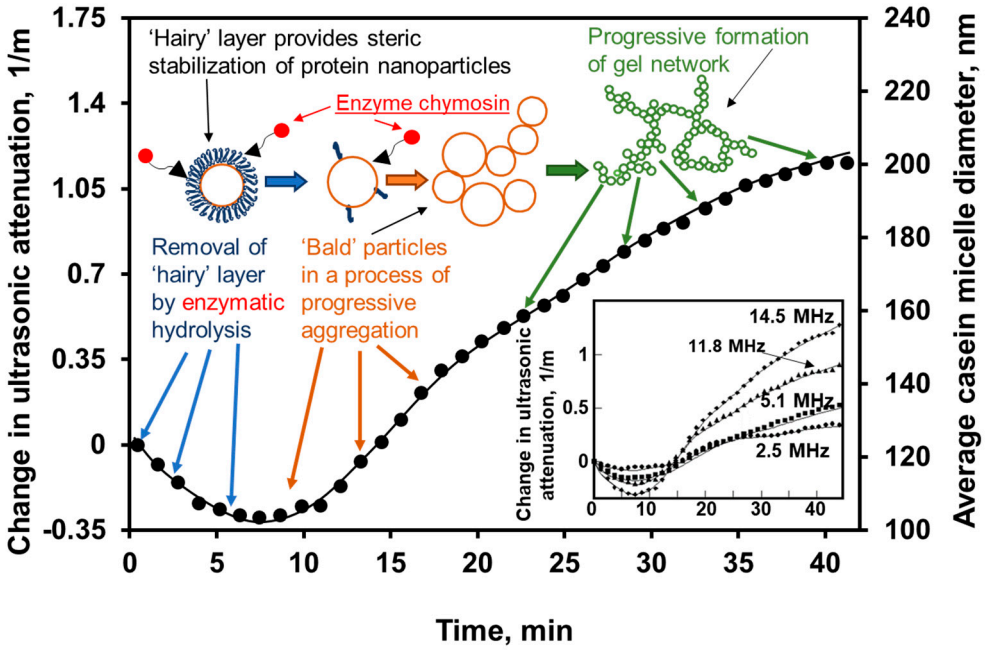

Figure 17. Ultrasonic real-time monitoring of evolution of size of protein nano particles during enzymatic 'haircut'.

Main frame. *Ultrasonic attenuation and particle size profile at 14.5 MHz in milk during enzymatic (chymosin) hydrolysis of the hairy layer of hydrated protein nanoparticles.*

Casein micelles, volume fraction 0.1 in milk at 30 °C. The average particle size was calculated using HR-US particle size software module.

Inset. *Effect of frequency on ultrasonic attenuation profiles of the hydrolysis.*

Measurements with HR-US 102 spectrometer (Ultrasonic Scientific, Dublin, Ireland). Adapted with permission from Reference [80]. Copyright © Proprietors of Journal of Dairy Research 2005.

9.2. Fast Chemical Kinetics

Figure 7C (inset) represents the attenuation profile of hydrolysis of peptide bonds of β-lactoglobulin (Reaction (R5)) catalyzed by protease α-chymotrypsin in 0.1 M phosphate buffer at pH 7.8) measured with HR-US 102 ultrasonic spectrometer using Procedure 1. As described in the Section 6.3 at pH 7.8 this reaction results in production of protonated, $-NH_3{}^+$, and deprotonated, $-NH_2$ terminal amino groups of oligopeptides. The ionization constant, pK_a, of these groups is 7.7 [84]. Consequently, these groups can participate in the reaction of proton transfer between them and the ions of the phosphate buffer: $-NH_3{}^+ + HPO_4{}^{-2} \rightleftharpoons -NH_2 + H_2PO_4{}^-$ [85–87]. Ionizable groups of amino acid side chains with pK_a values close to pH 7.8, which are exposed to contact with water as a result of hydrolysis, can also participate in the proton exchange with the ions of the phosphate buffer [85–87].

For common experimental conditions the relaxation frequency of the process of proton transfer is expected to be within low MHz range [85–89]. This agrees with our results presented in Figure 7C according to which at frequencies below 10 MHz (approximately) the amplitude of velocity rise during the process depends on the frequency, and a substantial increase of $\frac{\alpha}{f^2}$ during the reaction is observed. It is interesting to note that in contrary to the phosphate buffer, Tris, Bis-tris, Tes or Tricine and similar buffers do not show similar excessive attenuation in solutions of proteins at neutral pH in the low MHz frequency range [85]. When Equations (A11) and (A12) are considered, the observed frequency dependence of the rise of velocity and of $\frac{\alpha}{f^2}$ during the reaction indicates that the relaxation frequency f_{rel} of the proton transfer is at the lower side of the analyzed frequency range (2.7 MHz to 15.5 MHz),

or below it. At frequencies above 10 MHz (approximately), the frequency dependence of the rise of ultrasonic velocity and the amplitude of the rise of $\frac{\alpha}{f^2}$ vanish. At these high (relative to f_{rel}) frequencies, the relaxation process is 'frozen' as the period of oscillation of pressure and temperature in ultrasonic wave is significantly shorter than the relaxation time of the proton transfer. Although quantitative analysis of the evolution of frequency dependence of ultrasonic velocity and $\frac{\alpha}{f^2}$ during hydrolysis of β-lactoglobulin is outside of the scope of this paper, it shall be stated that such analysis provides new insights into the mechanisms of protein hydrolysis and can be used as a tool for real time monitoring of this reaction in phosphate buffer as well as real-time measurements of production of terminal amino groups of oligopeptides during hydrolysis of proteins.

Figure 5B illustrates the attenuation profile during the hydrolysis of maltodextrin. The decrease in attenuation cannot be explained only by the decrease in classical contribution to attenuation if 'low' frequency viscosities, η, of solutions maltodextrins maltodextrins [90–93] are applied to Equation (16). A relaxation process associated with conformational rearrangements within maltodextrins (see discussion of ultrasonic attenuation in aqueous solutions of carbohydrates in [94]) could be a reason for the observed attenuation decrease. Detailed analysis of this phenomenon shall provide additional capabilities for ultrasonic monitoring and analysis of hydrolysis of oligo and polysaccharides.

10. Conclusions

High-resolution ultrasonic spectroscopy can be successfully employed for real-time, non-destructive analysis of reactions catalyzed by enzymes and other catalysts in solutions and complex liquid dispersions. This technique provides precision reaction progress curves (concentration of reactant/product vs. time) over the whole course of reaction, and also can be utilized for analysis of structural rearrangements (change of particle size, aggregation) during reactions. It does not require optical transparency or optical markers and is applicable for reactions in continuous media and in micro/nano bioreactors (e.g., nanodroplets of microemulsions). The accuracy of commercial high-resolution ultrasonic spectrometers in measurements of change of ultrasonic velocity (down to 0.2 mm/s [23]) corresponds to μM level of precision in monitoring of the evolution of the concentrations of reactants and products [5,8,25]. This precision stands for mixtures with low and high concentration of substrates, which allows efficient assessment of stability of enzymes/catalysts and analysis of 'low yielding' reactions. The high precision can be used for measurements of the detailed 'reaction rate vs. concentration' profiles over the course of reaction, utilized in advanced modelling of reaction kinetics and inhibition effects. Other useful capabilities of the technique include measurements with programmable temperature profiles for assessments of reversible and non-reversible effects of thermal history on enzyme activity in a single sample. As ultrasonic measurements characterize the properties of the bulk medium, the unwanted effects of surfaces, often associated with reflectance spectroscopies and electrode techniques, are excluded. Since most of the chemical reactions in liquids are accompanied by hydration or solvation effects the described methodology should be applicable to a variety of reactions catalyzed by enzymes and other catalysts in various media. Importantly, the ultrasonic analysis can be carried out directly on intact samples with native substrates, thus allowing optimal application of catalysts in targeted media. Overall, the capabilities of this technique could make it a valuable tool in the field of catalysis based technologies.

Acknowledgments: We are grateful to Evgeny Koudryashov for his contribution with ultrasonic measurements of reactions of synthesis of ATP and hydrolysis of maltodextines, Shailesh Kumar for his contribution with ultrasonic measurements in microemulsions, Mark Dizon for his technical assistance, Rian Lynch for his assistance in editing the text, and to Sonas Technologies Ltd. for providing HR-US ultrasonic spectrometers, accessories and technical support. This research has been supported by 06RDTMFRC444 and 13F454 Grants from the Department of Agriculture, Food and the Marine of Ireland, MASF315 Grant from Science Foundation Ireland, H2020 EU Grant 690898 FORMILK, Postgraduate fellowship for Margarida Altas from School of Chemistry of University College Dublin.

Author Contributions: V.B. designed the structure and wrote the paper, M.C.A. contributed to data acquisition and data analysis, drafted the manuscript sections and prepared the figures. Both authors contributed to editing of the manuscript.

Conflicts of Interest: The authors declare no conflict of interest.

Appendix A.

Appendix A.1. Degree of Polymerization and Average Molar Mass

For a mixture of polymers consisting of monomers linked with the same covalent bond the average degree of polymerization, $\overline{DP}$, and the average molar mass, $\overline{M}$ are defined as:

$$\overline{DP} = \frac{\sum_{n=1}^{k} c_n n}{\sum_{n=1}^{k} c_n}; \; \overline{M} = \frac{\sum_{n=1}^{k} c_n M_n}{\sum_{n=1}^{k} c_n} \tag{A1}$$

where c_n is the concentration (number of moles in 1 kg of mixture) of molecules consisting of n monomeric units, M_n is their molar mass, and k is the maximum number of monomeric units in the polymer molecules. For linear polymers, the total concentration (number of moles in 1 kg of mixture) of bonds, $c_b(t)$, between the monomers at time t is given as:

$$c_b(t) = \sum_{n=1}^{k} c_n(n-1) = \sum_{n=1}^{k} c_n n - \sum_{n=1}^{k} c_n \tag{A2}$$

The total number of monomer units in all polymer molecules in 1 kg of the mixture, c_m, is given as:

$$c_m = \sum_{n=1}^{k} c_n n \tag{A3}$$

The parameter c_m is not affected by the breaking of the bonds between monomeric units within the molecules of polymer and, therefore, is constant over time. Following the above Equation (A2) can be rearranged as:

$$\sum_{n=1}^{k} c_n = c_m - c_b(t) \tag{A4}$$

The concentration $c_b(t)$ can be presented as:

$$c_b(t) = {c_b}^0 - c_{bh}(t) \tag{A5}$$

where ${c_b}^0$ is the concentration of the bonds at time zero ($t = 0$) and $c_{bh}(t)$ is the concentration of bonds broken during the time interval between time zero and time t. At $t = 0$ $c_{bh}(t) = 0$. Application of Equations (A3)–(A5) to the first of Equation (A1) results in:

$$\overline{DP} = \frac{\overline{DP}^0}{1 + c_{bh}(t)\frac{\overline{DP}^0 - 1}{{c_b}^0}} \tag{A6}$$

where $\overline{DP}^0$ is the average degree of polymerization at time zero ($t = 0$).

The sum $\sum_{n=1}^{k} c_n M_n$ in the second Equation (A1) represents the total mass of the molecules of the polymer in 1 kg of the mixture, which is the polymer weight fraction in the mixture, w_p:

$$\sum_{n=1}^{k} c_n M_n = w_p \tag{A7}$$

This and Equations (A1)–(A5) provide the following useful relationship:

$$\frac{\overline{DP}^0 - 1}{{c_b}^0} = \frac{\overline{M}^0}{{w_p}^0} \tag{A8}$$

where ${w_p}^0$ and $\overline{M}^0$ are the polymer weight fraction and the average molar mass at time zero ($t = 0$).

Derivation of an equivalent to Equation (A6) relationship for average molar mass, $\overline{M}$, requires an appropriate relationship between the weight fraction of polymer, w_p, and the concentration of bonds broken by the reaction, $c_{bh}(t)$. For reactions of hydrolysis, which are accompanied by a consumption of one mole of water molecule per one mole of bonds hydrolyzed, $w_p = {w_p}^0 + M_{H_2O} c_{bh}(t)$, where M_{H_2O} is the molar mass of water. Application of this relationship to Equations (A1)–(A5) and (A7) provides:

$$\overline{M} = \frac{\overline{M}^0 - M_{H_2O}}{1 + c_{bh}(t)\frac{\overline{M}^0}{{w_p}^0}} + M_{H_2O} \tag{A9}$$

For hydrolysis of polymers composed of the monomer units of the same molar mass the following relationship is correct $M_n = (M_1 - M_{H_2O})n + M_{H_2O}$, where M_1 is the molar mass of the free monomer. Application of this relationship to Equation (A1) results in:

$$\begin{aligned} \overline{M} &= (M_1 - M_{H_2O})\overline{DP} + M_{H_2O} \\ \overline{M}^0 &= (M_1 - M_{H_2O})\overline{DP}^0 + M_{H_2O} \end{aligned} \tag{A10}$$

These equations allow easy recalculations of the average degree of polymerization of such polymers to their average molar mass, which is especially useful for calculations of $\overline{DP}^0$ or $\overline{M}^0$.

Appendix A.2. Relaxation Contribution to Ultrasonic Velocity and Attenuation

For a relaxation process described by Reaction (R1) and characterized by the relaxation time τ, the contribution to attenuation caused by this process in dilute solutions is given by the following relationship [17,18]:

$$\frac{\alpha_{rel}}{f^2} = \frac{\pi\rho u}{RT}\frac{\Delta {V_S}^2 \Gamma}{f_{rel}}\frac{{f_{rel}}^2}{{f_{rel}}^2 + f^2} \tag{A11}$$

where R is the gas constant, $\Gamma = \left(\sum_{i=1}^{k}\frac{{a_i}^2}{c_{A_i}} + \sum_{i=1}^{l}\frac{{b_i}^2}{c_{B_i}}\right)^{-1}$ is the term representing the equilibrium concentrations of the reactants, c_{A_i}, and products, c_{B_i}, and the stoichiometric coefficients a_i and b_i of Reaction (R1), $f_{rel} = \frac{1}{2\pi\tau}$ is the relaxation frequency of the process, determined by the kinetic constants of the reaction and the concentrations of the reactants and products, ΔV_S is the volume effect of the reaction at adiabatic conditions given by: $\Delta V_S = \Delta V_T - \frac{e}{c_P}\Delta H$, where ΔV_T is the volume effect of the reaction (change of volume of the solution as a result of transferring of $a_1,\ a_2, \ldots, a_k$ moles of reactants $A_1,\ A_2, \ldots, A_k$ to $b_1,\ b_2, \ldots, b_k$ moles of products $B_1,\ B_2, \ldots, B_k$) at constant temperature and

ΔH is the enthalpy of reaction. The contribution of the relaxation process to ultrasonic velocity, u_{rel}, at $|u_{rel}| \ll u$ (e.g., dilute solution) is given as:

$$u_{rel} = -\frac{\rho u^3}{2RT}\Delta V_S{}^2\Gamma\frac{f_{rel}{}^2}{f_{rel}{}^2+f^2} = -\frac{f_{rel}u^2}{2\pi}\frac{\alpha_{rel}}{f^2} \quad \text{(A12)}$$

According to Equations (A11) and (A12) the relaxation contribution $\frac{\alpha_{rel}}{f^2}$ is positive and the contribution u_{rel} is negative. The dependencies of both contributions on the frequency have an S-shape profile with plateaus at low ($f \ll f_{rel}$) and high ($f \gg f_{rel}$) frequencies and half transition point at $f = f_{rel}$. At measuring frequencies significantly lower than f_{rel} the relaxation contribution to the ultrasonic attenuation is given as $\frac{\alpha_{rel}}{f^2} = \frac{\pi\rho u}{RT}\frac{\Delta V_S{}^2\Gamma}{f_{rel}}$ and to the ultrasonic velocity as $u_{rel} = -\frac{\rho u^3}{2RT}\Delta V_S{}^2\Gamma$. At frequencies close to f_{rel} the absolute value of both contributions decreases with frequency and vanish at frequencies far above f_{rel}. At these high frequencies, the relaxation process is 'frozen' as its relaxation time is much longer than the period of oscillations of pressure and temperature in the ultrasonic wave.

Appendix A.3. Ultrasonic Particle Sizing

Heterogeneous dispersions produce 'scattering' contribution to ultrasonic velocity and attenuation, which is a function of the particle's size and the volume fraction [95–98]. Generally, analysis of the scattering from particles requires numerical solutions. Nevertheless, in the long wavelength regime, (i.e., when the wavelength of ultrasound is much longer than the particle radius), explicit expressions for the ultrasonic scattering in dispersions could be utilized [99]. The basic mechanism of the interaction of ultrasonic wave with particles in dispersions in this regime can be illustrated with two major scattering contributions, thermoelastic and viscoinertial [22,99]. These contributions result from the 'scattering' of the incident ultrasonic waves into the thermal and viscous waves on the border between the particle and the continuous medium. The thermoelastic and viscoinertial mechanisms normally dominate the scattering contribution to ultrasonic attenuation in dispersions of micron and submicron size range and for the operational frequency range of high-resolution ultrasonic spectrometers (1 to 20 MHz). For the long wavelength regime, the approximation formulas describing the ultrasonic velocity and attenuation in dispersions of spherical particles can be presented as [100,101]:

$$K^2 = k_1{}^2\left(1-\frac{3\phi i B_0}{k_1{}^3r^3}\right)\left(1-\frac{9\phi i B_1}{k_1{}^3r^3}\right) \quad \text{(A13)}$$

where:

$K = \frac{\omega}{u} + i\alpha$ is a complex propagation constant of the dispersion,
u is the ultrasonic velocity and α is the ultrasonic attenuation coefficient in the dispersion,
ϕ is the volume fraction of the dispersed phase,
$i = \sqrt{-1}$,
r is the particle radius,
$\omega = 2\pi f$ is the angular frequency, f is the ultrasonic frequency,
$k_1 = \frac{\omega}{u_1} + i\alpha_1$ is the complex propagation constant of the continuous phase,
u_1 is the ultrasonic velocity and α_1 is the attenuation in the continuous phase,
$B_0 = \frac{ik_1{}^3r^3}{3}\left(\frac{\rho_1 k_2{}^2}{\rho_2 k_1{}^2}-1\right) - \frac{ik_1{}^3r^3\xi H}{z_1{}^2}\left(1-\frac{\beta_2\rho_1 c_{p1}}{\beta_1\rho_2 c_{p2}}\right)^2$,
$B_1 = \frac{-ik_1^3r^3}{9}\left(\frac{(\rho_1-\rho_2)(1+T_v+is)}{(\rho_2+\rho_1 T_v+i\rho_1 s)}\right)$,
$\frac{1}{H} = \frac{1}{(1-iz_1)} - \frac{\kappa_1}{\kappa_2}\frac{\tan(z_2)}{\tan(z_2)-z_2}$,
$s = \frac{9\delta}{4r}\left(1+\frac{\delta}{r}\right)$,

$T_\nu = \frac{1}{2} + \frac{9\delta}{4r}$,
$z_1 = (1+i)\frac{r}{\delta_1}, z_2 = (1+i)\frac{r}{\delta_2}$,
$\xi = \frac{T\beta_1{}^2 u_1{}^2}{c_{p1}}$,
$\delta = \sqrt{\frac{2\eta_1}{\omega\rho_1}}$, $\delta_1 = \sqrt{\frac{2\kappa_1}{\omega c_{p1}\rho_1}}$, $\delta_2 = \sqrt{\frac{2\kappa_2}{\omega c_{p2}\rho_2}}$,
$k_2 = \frac{\omega}{u_2} + i\alpha_2$ is the complex propagation constant of the dispersed phase,
u_2 is the ultrasonic velocity and α_2 is the attenuation coefficient in the dispersed phase,
η_1 is the viscosity of the continuous phase,
$\beta_1 = \rho_1 e_1$, $\beta_2 = \rho_2 e_2$ are the coefficients of volume expansion for the continuous phase and the dispersed phase,
c_{p1}, c_{p2} are the specific heat capacities of the continuous and dispersed phase at constant pressure,
ρ_1, ρ_2 are the densities of the continuous and dispersed phases,
κ_1, κ_2 are thermal conductivities of the continuous and dispersed phases,
T is temperature in K.

Appendix A.4. Materials and Instruments Utilized in Previously Unpublished Illustrations

All aqueous solutions were prepared by weight using purified water (Milli-Q gradient ultrapure purification system, conductivity 0.056 µS/cm, resistivity 18 MΩ cm, TOC max. value 100 µg/L). Phosphate buffers were prepared from dibasic (anhydrous BioUltra cat. 60353) and monobasic (anhydrous BioUltra cat. 60218) potassium phosphate.

Ultrasonic measurements were performed with HR-US 102 range spectrometers and their accessories from Sonas Technologies Ltd. (Dublin, Ireland).

Figures 3 and 7.

β-lactoglobulin from bovine milk from Sigma-Aldrich Co. (St. Louis, MO, USA), cat. L3908, lyophilized powder. α-chymotrypsin from bovine pancreas, Sigma-Aldrich Co, cat. C3142, Type VII, lyophilized powder, with a declared activity of ≥64 U/mg protein. 2,4,6-Trinitrobenzenesulfonic acid (TNBS) from Sigma-Aldrich Co., cat. P2297.

Figures 3 and 8.

ADP, adenosine 5′-diphosphate sodium salt, from Sigma-Aldrich Co., cat. A2754. Phosphocreatine disodium salt hydrate from Sigma-Aldrich Co., cat. P7936. Creatine phosphokinase from rabbit muscle, Sigma-Aldrich Co., cat. C3755, type I, lyophilized powder, with a declared activity of ≥150 U/mg protein. Gly-gly (diglycine) from Sigma-Aldrich Co., cat. G1002, BSA from Sigma-Aldrich Co., cat. B4287. Magnesium acetate Sigma-Aldrich Co., cat. 22864-8.

Figures 5 and 11.

Maltodextrin from Sigma-Aldrich Co., cat. 419680, 14.5 dextrose equivalents (corresponds to average degree of polymerization 7.55). α-amylase from *Bacillus* sp., Sigma-Aldrich Co., cat. A6380, Type II-A, lyophilized powder, with a declared activity of 2680 U/mg protein, concentration 0.016 g/L. BCA assay: Bicinchoninic acid (4,4′-dicarboxy-2,2′-biquinoline) from Sigma-Aldrich Co., cat. 391778; Na_2CO_3 anhydrous powder from Sigma-Aldrich Co., cat. 451614; aspartic acid from Sigma-Aldrich Co., cat. A93100; $CuSO_4$ anhydrous powder from Sigma-Aldrich Co. cat. 451657.

References

1. Hall, A.M.; Chouler, J.C.; Codina, A.; Gierth, P.T.; Lowe, J.P.; Hintermair, U. Practical aspects of real-time reaction monitoring using multi-nuclear high resolution FlowNMR spectroscopy. *Catal. Sci. Technol.* **2016**, *6*, 8406–8417. [CrossRef]
2. Kudryashov, E.; Smyth, C.; O'Driscoll, B.; Buckin, V. High-Resolution Ultrasonic Spectroscopy for analysis of chemical reactions in real time. *Spectroscopy* **2003**, *18*, 26–32.

3. Danieli, E.; Perlo, J.; Duchateau, A.; Verzijl, G.; Litvinov, V.; Blümich, B.; Casanova, F. On-Line Monitoring of Chemical Reactions by using Bench-Top Nuclear Magnetic Resonance Spectroscopy. *ChemPhysChem* **2014**, *15*, 3060–3066. [CrossRef] [PubMed]
4. Bernstein, M.A.; Štefinović, M.; Sleigh, C.J. Optimising reaction performance in the pharmaceutical industry by monitoring with NMR. *Magn. Reson. Chem.* **2007**, *45*, 564–571. [CrossRef] [PubMed]
5. Li, Y.; Buckin, V. Ultrasonic real-time monitoring of the process of decomposition of hydrogen peroxide in aqueous solutions. *Anal. Methods* **2016**, *8*, 4828–4834. [CrossRef]
6. Baltes, W. *Rapid Methods for Analysis of Food and Food Raw Material*; Behr's Verlag: Hamburg, Germany, 1990.
7. Wiss, J.; Länzlinger, M.; Wermuth, M. Safety improvement of a Grignard reaction using on-line NIR monitoring. *Org. Process Res. Dev.* **2005**, *9*, 365–371. [CrossRef]
8. Caras Altas, M.; Kudryashov, E.; Buckin, V. Ultrasonic monitoring of enzyme catalysis. Enzyme activity in formulations for lactose intolerant infants. *Anal. Chem.* **2016**, *88*, 4714–4723. [CrossRef] [PubMed]
9. Wahler, D.; Reymond, J.-L. Novel methods for biocatalyst screening. *Curr. Opin. Chem. Biol.* **2001**, *5*, 152–158. [CrossRef]
10. Bothner, B.; Chavez, R.; Wei, J.; Strupp, C.; Phung, Q.; Schneemann, A.; Siuzdak, G. Monitoring enzyme catalysis with mass spectrometry. *J. Biol. Chem.* **2000**, *275*, 13455–13459. [CrossRef] [PubMed]
11. Mello, L.D.; Kubota, L.T. Review of the use of biosensors as analytical tools in the food and drink industries. *Food Chem.* **2002**, *77*, 237–256. [CrossRef]
12. Povey, M.J.; Mason, T.J. *Ultrasound in Food Processing*; Springer: Berlin, Germany, 1998.
13. Buckin, V. Application of High-Resolution Ultrasonic Spectroscopy for analysis of complex formulations. Compressibility of solutes and solute particles in liquid mixtures. *IOP Conf. Ser. Mater. Sci. Eng.* **2012**, *42*, 1–18. [CrossRef]
14. Holmes, M.; Povey, M. Ultrasonic Particle Sizing in Emulsions. *Ultrasound Food Proc. Recent Adv.* **2017**, 27–64. [CrossRef]
15. Kaatze, U.; Eggers, F.; Lautscham, K. Ultrasonic velocity measurements in liquids with high resolution—Techniques, selected applications and perspectives. *Meas. Sci. Technol.* **2008**, *19*, 1–21. [CrossRef]
16. Buckin, V.; Kudryashov, E.; O'Driscoll, B. An alternative spectroscopy technique for biopharmaceutical applications. *Pharm. Technol. Eur.* **2002**, *14*, 33–37.
17. Eigen, M.; De Maeyer, L. *Techniques of Organic Chemistry*; Friess, S.L., Lewis, E.S., Weisberger, A., Eds.; Investigation of Rates and Mechanisms of Reactions; Relaxation Methods Interscience: New York, NY, USA, 1963; Volume 8.
18. Stuehr, J.; Yeager, E. *Physical Acoustics*; Mason, W.P., Ed.; Academic Press: New York, NY, USA, 1965; Volume 2.
19. Smyth, C.; Kudryashov, E.; O'Driscoll, B.; Buckin, V. High-resolution ultrasonic spectroscopy for analysis of industrial emulsions and suspensions. *JALA J. Assoc. Lab. Autom.* **2004**, *9*, 87–90. [CrossRef]
20. Holmes, M.; Southworth, T.; Watson, N.; Povey, M. *Enzyme Activity Determination Using Ultrasound*; IOP Publishing: Bristol, UK, 2014; p. 012003.
21. Resa, P.; Elvira, L.; De Espinosa, F.M.; Gómez-Ullate, Y. Ultrasonic velocity in water–ethanol–sucrose mixtures during alcoholic fermentation. *Ultrasonics* **2005**, *43*, 247–252. [CrossRef] [PubMed]
22. Povey, M.J. *Ultrasonic Techniques for Fluids Characterization*; Academic Press Limited: London, UK, 1997.
23. Buckin, V.; O'Driscoll, B. Ultrasonic waves and material analysis: Recent advances and future trends. *LabPlus Int.* **2002**, *16*, 17–21.
24. Buckin, V.; Smyth, C. High-resolution ultrasonic resonator measurements for analysis of liquids. *Semin. Food Anal.* **1999**, *4*, 113–130.
25. Resa, P.; Buckin, V. Ultrasonic analysis of kinetic mechanism of hydrolysis of cellobiose by beta-glucosidase. *Anal. Biochem.* **2011**, *415*, 1–11. [CrossRef] [PubMed]
26. Niemeyer, K. Ultrasonic Methods for Analytical Determination of Pancreatic Enzyme Activities in Pharmaceutical Preparations. Ph.D. Thesis, PHD Thesis Fakultät für Lebenswissenschaften der Technischen Universität Carolo-Wilhelmina, Braunschweig, Germany, 2012.
27. Jager, M.; Kaatze, U.; Kudryashov, E.; O'Driscoll, B.; Buckin, V. New capabilities of high-resolution ultrasonic spectroscopy: Titration analysis. *Sperctoscopy* **2005**, *20*, 20–26.
28. Van Durme, K.; Delellio, L.; Kudryashov, E.; Buckin, V.; Van Mele, B. Exploration of high-resolution ultrasonic spectroscopy as an analytical tool to study demixing and remixing in poly(*N*-isopropyl acrylamide)/water solutions. *J. Polym. Sci. Part B Polym. Phys.* **2005**, *43*, 1283–1295. [CrossRef]

29. Hickey, S.; Lawrence, M.J.; Hagan, S.A.; Buckin, V. Analysis of the phase diagram and microstructural transitions in phospholipid microemulsion systems using high-resolution ultrasonic spectroscopy. *Langmuir* **2006**, *22*, 5575–5583. [CrossRef] [PubMed]
30. Hickey, S.; Hagan, S.A.; Kudryashov, E.; Buckin, V. Analysis of phase diagram and microstructural transitions in an ethyl oleate/water/Tween 80/Span 20 microemulsion system using high-resolution ultrasonic spectroscopy. *Int. J. Pharm.* **2010**, *388*, 213–222. [CrossRef] [PubMed]
31. Buckin, V.; Hallone, S.K. Ultrasonic Characterisation of W/O Microemulsions—Structure, Phase Diagrams, State of Water in Nano–Droplets, Encapsulated Proteins, Enzymes. In *Microemulsions—An Introduction to Properties and Applications*; InTech: London, UK, 2012; pp. 33–66.
32. Bainor, A.; Chang, L.; McQuade, T.J.; Webb, B.; Gestwicki, J.E. Bicinchoninic acid (BCA) assay in low volume. *Anal. Biochem.* **2011**, *410*, 310–312. [CrossRef] [PubMed]
33. Johnston, D.; Shoemaker, S.; Smith, G.; Whitaker, J. Kinetic measurements of cellulase activity on insoluble substrates using disodium 2, 2′ bicinchoninate. *J. Food Biochem.* **1998**, *22*, 301–319. [CrossRef]
34. Adler-Nissen, J. Determination of the Degree of Hydrolysis of Food Protein Hydrolysates by Trinitrobenzenesulfonic Acid. *J. Agric. Food Chem.* **1979**, *27*, 1256–1262. [CrossRef] [PubMed]
35. Kharakoz, D.P. Partial Volumes and Compressibilities of Extended Polypeptide Chains in Aqueous Solution: Additivity Scheme and Implication of Protein Unfolding at Normal and High Pressure. *Biochemistry* **1997**, *36*, 10276–10285. [CrossRef] [PubMed]
36. Vorob'ev, M.; Levicheva, I.Y.; Belikov, V. Kinetics of the initial stage of milk protein hydrolysis by chymotrypsin. *Appl. Biochem. Microbiol.* **1996**, *32*, 219–222.
37. Goncharova, I. Computer simulation of proteolysis. Peptic hydrolysis of partially demasked β-Lactoglobulin. *Mol. Nutr. Food Res.* **1998**, *42*, 61–67.
38. Nihei, T.; Noda, L.; Morales, M.F. Kinetic Properties and Equilibrium Constant of the Adenosine Triphosphate-Creatine Transphosphorylase-catalyzed Reaction. *J. Biol. Chem.* **1961**, *236*, 3203–3209. [PubMed]
39. Pierce, A.D. *Acoustics: An Introduction to Its Physical Principles and Applications*; American Institute of Physics: New York, NY, USA, 1989.
40. Litovitz, T.A.; Davis, C.M. *Physical Acoustics*; Mason, W.P., Ed.; Academic Press: New York, NY, USA, 1964; Volume 2.
41. Ochenduszko, A.; Buckin, V. Real-time monitoring of heat-induced aggregation of β-lactoglobulin in aqueous solutions using high-resolution ultrasonic spectroscopy. *Int. J. Thermophys.* **2010**, *31*, 113–130. [CrossRef]
42. Hoshino, E.; Tanaka, A.; Kanda, T. Effects of a nonionic surfactant on the behavior of Bacillus amyloliquefaciens α-amylase in the hydrolysis of malto-oligosaccharide. *J. Surfactants Deterg.* **2006**, *9*, 63–68. [CrossRef]
43. Robyt, J.; French, D. Action pattern and specificity of an amylase from Bacillus subtilis. *Arch. Biochem. Biophys.* **1963**, *100*, 451–467. [CrossRef]
44. Yook, C.; Robyt, J.F. Reactions of alpha amylases with starch granules in aqueous suspension giving products in solution and in a minimum amount of water giving products inside the granule. *Carbohydr. Res.* **2002**, *337*, 1113–1117. [CrossRef]
45. Rodriguez-Colinas, B.; Fernandez-Arrojo, L.; Ballesteros, A.; Plou, F. Galactooligosaccharides formation during enzymatic hydrolysis of lactose: Towards a prebiotic-enriched milk. *Food Chem.* **2014**, *145*, 388–394. [CrossRef] [PubMed]
46. Jurado, E.; Camacho, F.; Luzon, G.; Vicaria, J.M. Kinetic models of activity for beta-galactosidases: Influence of pH, ionic concentration and temperature. *Enzyme Microb. Technol.* **2004**, *34*, 33–40. [CrossRef]
47. Martínez-Villaluenga, C.; Cardelle-Cobas, A.; Corzo, N.; Olano, A.; Villamiel, M. Optimization of conditions for galactooligosaccharide synthesis during lactose hydrolysis by β-galactosidase from Kluyveromyces lactis (Lactozym 3000 L HP G). *Food Chem.* **2008**, *107*, 258–264. [CrossRef]
48. Roefs, P.; de Kruif, K.G. Association behavior of native ß-lactoglobulin. *Biopolymers* **1999**, *49*, 11–20.
49. Berg, J.M.; Tymoczko, T.J.; Stryer, L. Catalytic Strategies. In *Biochemistry*; WH Freeman and Company: New York, NY, USA, 2007; pp. 241–274.
50. Lisak, K.; Toro-Sierra, J.; Kulozik, U.; Božanić, R.; Cheison, S.C. Chymotrypsin selectively digests β-lactoglobulin in whey protein isolate away from enzyme optimal conditions: Potential for native α-lactalbumin purification. *J. Dairy Res.* **2013**, *80*, 14–20. [CrossRef] [PubMed]

51. Maria, C.; Galvão, A.; Silva, A.F.S.; Custódio, M.F.; Monti, R.; De, R.; Giordano, C. Controlled hydrolysis of cheese whey proteins using trypsin and [alpha]-chymotrypsin. *Appl. Biochem. Biotechnol.* **2001**, *91*, 761–776.
52. Brot, F.E.; Bender, M.L. Use of the specificity constant of. alpha.-chymotrypsin. *J. Am. Chem. Soc.* **1969**, *91*, 7187–7191. [CrossRef]
53. Chae, H.J.; In, M.-J.; Kim, M.-H. Process development for the enzymatic hydrolysis of food protein: Effects of pre-treatment and post-treatments on degree of hydrolysis and other product characteristics. *Biotechnol. Bioprocess Eng.* **1998**, *3*, 35–39. [CrossRef]
54. Clemente, A. Enzymatic protein hydrolysates in human nutrition. *Trends Food Sci. Technol.* **2000**, *11*, 254–262. [CrossRef]
55. Korhonen, H. Milk-derived bioactive peptides: From science to applications. *J. Funct. Foods* **2009**, *1*, 177–187. [CrossRef]
56. Dawson, D.M. Creatine kinase from brain: Kinetic aspects. *J. Neurochem.* **1970**, *17*, 65–74. [CrossRef] [PubMed]
57. Tanzer, M.L.; Gilvarg, C. Creatine and Creatine Kinase Measurement. *J. Biol. Chem.* **1959**, *234*, 3201–3204. [PubMed]
58. Lin, S.-S.; Gurol, M.D. Catalytic Decomposition of Hydrogen Peroxide on Iron Oxide: Kinetics, Mechanism, and Implications. *Environ. Sci. Technol.* **1998**, *32*, 1417–1423. [CrossRef]
59. Watts, R.J.; Foget, M.K.; Kong, S.-H.; Teel, A.L. Hydrogen peroxide decomposition in model subsurface systems. *J. Hazard. Mater.* **1999**, *69*, 229–243. [CrossRef]
60. Petri, B.G.; Watts, R.J.; Teel, A.L.; Huling, S.G.; Brown, R.A. Fundamentals of ISCO Using Hydrogen Peroxide. In *In Situ Chemical Oxidation for Groundwater Remediation*; Siegrist, R.L., Crimi, M., Simpkin, T.J., Eds.; Springer: New York, NY, USA, 2011; pp. 33–88.
61. Zepp, R.G.; Faust, B.C.; Hoigne, J. Hydroxyl radical formation in aqueous reactions (pH 3–8) of iron(II) with hydrogen peroxide: The photo-Fenton reaction. *Environ. Sci. Technol.* **1992**, *26*, 313–319. [CrossRef]
62. Kwan, W.P.; Voelker, B.M. Decomposition of Hydrogen Peroxide and Organic Compounds in the Presence of Dissolved Iron and Ferrihydrite. *Environ. Sci. Technol.* **2002**, *36*, 1467–1476. [CrossRef] [PubMed]
63. Chu, L.; Wang, J.; Dong, J.; Liu, H.; Sun, X. Treatment of coking wastewater by an advanced Fenton oxidation process using iron powder and hydrogen peroxide. *Chemosphere* **2012**, *86*, 409–414. [CrossRef] [PubMed]
64. Chakinala, A.G.; Bremner, D.H.; Gogate, P.R.; Namkung, K.-C.; Burgess, A.E. Multivariate analysis of phenol mineralisation by combined hydrodynamic cavitation and heterogeneous advanced Fenton processing. *Appl. Catal. B Environ.* **2008**, *78*, 11–18. [CrossRef]
65. Doong, R.-A.; Chang, W.-H. Photodegradation of parathion in aqueous titanium dioxide and zero valent iron solutions in the presence of hydrogen peroxide. *J. Photochem. Photobiol. A Chem.* **1998**, *116*, 221–228. [CrossRef]
66. Bremner, D.H.; Burgess, A.E.; Houllemare, D.; Namkung, K.-C. Phenol degradation using hydroxyl radicals generated from zero-valent iron and hydrogen peroxide. *Appl. Catal. B Environ.* **2006**, *63*, 15–19. [CrossRef]
67. Kolisis, F.N.; Stamatis, H.; Flickinger, M.C. Reverse Micelles, Enzymes. In *Encyclopedia of Industrial Biotechnology*; John Wiley & Sons, Inc.: Hoboken, NJ, USA, 2009.
68. Stamatis, H.; Xenakis, A.; Kolisis, F.N. Bioorganic reactions in microemulsions: The case of lipases. *Biotechnol. Adv.* **1999**, *17*, 293–318. [CrossRef]
69. Smyth, C.; O'Driscoll, B.; Lawrence, J.; Hickey, S.; O'Reagan, T.; Buckin, V. High-Resolution Ultrasonic Spectroscopy Analysis of Microemulsions. *Pharm. Technol. Eur.* **2004**, *16*, 31–34.
70. Tonova, K.; Lazarova, Z. Reversed micelle solvents as tools of enzyme purification and enzyme-catalyzed conversion. *Biotechnol. Adv.* **2008**, *26*, 516–532. [CrossRef] [PubMed]
71. Maruhenda-Egea, F.C.; Piera-Vélasquez, S.; Cadenas, C.; Cadenas, E. Reverse micelles in organic solvents: A medium for the biotechnological use of extreme halophilic enzymes at low salt concentration. *Archaea* **2002**, *1*, 105–111. [CrossRef]
72. Dorovska-Taran, V.; Veeger, C.; Visser, A.J.W.G. Reverse micelles as a water-property-control system to investigate the hydration/activity relationship of α-chymotrypsin. *Eur. J. Biochem.* **1993**, *218*, 1013–1019. [CrossRef] [PubMed]
73. Panintrarux, C.; Adachi, S.; Araki, Y.; Kimura, Y.; Matsuno, R. Equilibrium yield of n-alkyl-β-D-glucoside through condensation of glucose and n-alcohol by β-glucosidase in a biphasic system. *Enzyme Microb. Technol.* **1995**, *17*, 32–40. [CrossRef]

74. Kouptsova, O.S.; Klyachko, N.L.; Levashov, A.V. Synthesis of Alkyl Glycosides Catalyzed by β-Glycosidases in a System of Reverse Micelles. *Russian J. Bioorganic Chem.* **2001**, *27*, 380–384. [CrossRef]
75. Grous, W.; Converse, A.; Grethlein, H.; Lynd, L. Kinetics of cellobiose hydrolysis using cellobiase composites from *Ttrichoderma reesei* and *Aspergillus niger*. *Biotechnol. Bioeng.* **1985**, *27*, 463–470. [CrossRef] [PubMed]
76. Gong, C.-S.; Ladisch, M.R.; Tsao, G.T. Cellobiase from Trichoderma viride: Purification, properties, kinetics, and mechanism. *Biotechnol. Bioeng.* **1977**, *19*, 959–981. [CrossRef] [PubMed]
77. Segel, I.H. *Enzyme Kinetics: Behavior and Analysis of Rapid Equilibrium and Steady-State Enzyme Systems*; Wiley: Hoboken, NJ, USA, 1993.
78. Boy, M.; Dominik, A.; Voss, H. Fast determination of biocatalyst process stability. *Process Biochem.* **1999**, *34*, 535–547. [CrossRef]
79. Neri, D.F.; Balcão, V.M.; Carneiro-da-Cunha, M.G.; Carvalho, L.B., Jr.; Teixeira, J.A. Immobilization of β-galactosidase from Kluyveromyces lactis onto a polysiloxane–polyvinyl alcohol magnetic (mPOS–PVA) composite for lactose hydrolysis. *Catal. Commun.* **2008**, *9*, 2334–2339. [CrossRef]
80. Dwyer, C.; Donnelly, L.; Buckin, V. Ultrasonic analysis of rennet-induced pre-gelation and gelation processes in milk. *J. Dairy Res.* **2005**, *72*, 303–310. [CrossRef] [PubMed]
81. Lehmann, L.; Buckin, V. Determination of the Heat Stability Profiles of Concentrated Milk and Milk Ingredients Using High Resolution Ultrasonic Spectroscopy. *J. Dairy Sci.* **2005**, *88*, 3121–3129. [CrossRef]
82. Griffin, W.G.; Griffin, M.C.A. The attenuation of ultrasound in aqueous suspensions of casein micelles from bovine milk. *J. Acoust. Soc. Am.* **1990**, *87*, 2541–2550. [CrossRef]
83. Holt, C.; Dalgleish, D.G. Electrophoretic and hydrodynamic properties of bovine casein micelles interpreted in terms of particles with an outer hairy layer. *J. Colloid Interface Sci.* **1986**, *114*, 513–524. [CrossRef]
84. Adler-Nissen, J. *Enzymic Hydrolysis of Food Proteins*; Elsevier Applied Science Publishers Ltd.: Amsterdam, The Netherlands, 1986.
85. Jürgens, K.D.; Baumann, R. Ultrasonic absorption studies of protein-buffer interactions. *Eur. Biophys. J.* **1985**, *12*, 217–222. [CrossRef] [PubMed]
86. Slutsky, L.; Madsen, L.; White, R. Acoustic absorption and proton-exchange kinetics in aqueous bovine pancreatic ribonuclease A. *J. Phys. Chem.* **1984**, *88*, 5679–5683. [CrossRef]
87. Slutsky, L.; Madsen, L.; White, R.; Harkness, J. Kinetics of the exchange of protons between hydrogen phosphate ions and a histidyl residue. *J. Phys. Chem.* **1980**, *84*, 1325–1329. [CrossRef]
88. Rogez, D.; Cerf, R.; Andrianjara, R.; Salehi, S.-T.; Fouladgar, H. Ultrasonic studies of proton-transfer reactions at the catalytic site of α-chymotrypsin. *FEBS Lett.* **1987**, *219*, 22–26. [CrossRef]
89. Strom-Jensen, P.R.; Dunn, F. Ultrasonic absorption by solvent–solute interactions and proton transfer in aqueous solutions of peptides and small proteins. *J. Acoust. Soc. Am.* **1984**, *75*, 960–966. [CrossRef]
90. Johnson, J.; Srisuthep, R. Physical and chemical properties of oligosaccharides. *Cereal Chem.* **1975**, *52*, 70–78.
91. Chirife, J.; Buera, M. A simple model for predicting the viscosity of sugar and oligosaccharide solutions. *J. Food Eng.* **1997**, *33*, 221–226. [CrossRef]
92. Avaltroni, F.; Bouquerand, P.; Normand, V. Maltodextrin molecular weight distribution influence on the glass transition temperature and viscosity in aqueous solutions. *Carbohydr. Polym.* **2004**, *58*, 323–334. [CrossRef]
93. Dokic, P.; Jakovljevic, J.; Dokic-Baucal, L. Molecular characteristics of maltodextrins and rheological behaviour of diluted and concentrated solutions. *Colloids Surf. A Physicochem. Eng. Asp.* **1998**, *141*, 435–440. [CrossRef]
94. Kaatze, U.; Hushcha, T.; Eggers, F. Ultrasonic Broadband Spectrometry of Liquids A Research Tool in Pure and Applied Chemistry and Chemical Physics. *J. Solut. Chem.* **2000**, *29*, 299–368. [CrossRef]
95. Epstein, P.S.; Carhart, R.R. The absorption of sound in suspensions and emulsions. I. Water fog in air. *J. Acoust. Soc. Am.* **1953**, *25*, 553–565. [CrossRef]
96. Waterman, P.C.; Truell, R. Multiple scattering of waves. *J. Math. Phys.* **1961**, *2*, 512–537. [CrossRef]
97. Fikioris, J.; Waterman, P. Multiple Scattering of Waves. II. "Hole Corrections" in the Scalar Case. *J. Math. Phys.* **1964**, *5*, 1413–1420. [CrossRef]
98. Lloyd, P.; Berry, M. Wave propagation through an assembly of spheres: IV. Relations between different multiple scattering theories. *Proc. Phys. Soc.* **1967**, *91*, 678. [CrossRef]
99. Allegra, J.; Hawley, S. Attenuation of sound in suspensions and emulsions: Theory and experiments. *J. Acoust. Soc. Am.* **1972**, *51*, 1545–1564. [CrossRef]

100. McClements, D.; Coupland, J. Theory of droplet size distribution measurements in emulsions using ultrasonic spectroscopy. *Colloids Surf. A Physicochem. Eng. Asp.* **1996**, *117*, 161–170. [CrossRef]
101. McClements, D.J.; Hemar, Y.; Herrmann, N. Incorporation of thermal overlap effects into multiple scattering theory. *J. Acoust. Soc. Am.* **1999**, *105*, 915–918. [CrossRef]